

# Inducible miR-1224 silences cerebrovascular *Serpine1* and restores blood flow to the stroke-affected site of the brain

Ravichand Palakurti,<sup>1</sup> Nirupam Biswas,<sup>1</sup> Sashwati Roy,<sup>1</sup> Surya C. Gnyawali,<sup>1</sup> Mithun Sinha,<sup>1</sup> Kanhaiya Singh,<sup>1</sup> Subhadip Ghatak,<sup>1</sup> Chandan K. Sen,<sup>1,2</sup> and Savita Khanna<sup>1</sup>

<sup>1</sup>Department of Surgery, Indiana Center for Regenerative Medicine and Engineering, Indiana University School of Medicine, Indianapolis, IN 46202, USA; <sup>2</sup>Weldon School of Biomedical Engineering, Purdue University, West Lafayette, IN, USA

**The  $\alpha$ -tocotrienol (TCT) form of natural vitamin E is more potent than the better known  $\alpha$ -tocopherol against stroke. Angiographic studies of canine stroke have revealed beneficial cerebrovascular effects of TCT. This work seeks to understand the molecular basis of such effect. In mice, TCT supplementation improved perfusion at the stroke-affected site by inducing miR-1224. miRNA profiling of a laser-capture-microdissected stroke-affected brain site identified miR-1224 as the only vascular miR induced. Lentiviral knockdown of miR-1224 significantly blunted the otherwise beneficial effects of TCT on stroke outcomes. Studies on primary brain microvascular endothelial cells revealed direct angiogenic properties of miR-1224. In mice not treated with TCT, advance stereotaxic delivery of an miR-1224 mimic to the stroke site markedly improved stroke outcomes. Mechanistic studies identified *Serpine1* as a target of miR-1224. Downregulation of *Serpine1* augmented the angiogenic response of the miR-1224 mimic in the brain endothelial cells. The inhibition of *Serpine1*, by dietary TCT and pharmacologically, increased cerebrovascular blood flow at the stroke-affected site and protected against stroke. This work assigns *Serpine1*, otherwise known to be of critical significance in stroke, a cerebrovascular function that worsens stroke outcomes. miR-1224-dependent inhibition of *Serpine1* can be achieved by dietary TCT as well as by the small-molecule inhibitor TM5441.**

## INTRODUCTION

Ischemic stroke is the fifth leading cause of death and cognitive impairment in the United States.<sup>1</sup> Ischemic stroke causes severe reduction of cerebral blood flow resulting in a lack of oxygen and nutrients, which leads to neuronal cell death and infarction at the affected site of the brain.<sup>2</sup> Two decades ago, our laboratory identified that, on a concentration basis, the  $\alpha$ -tocotrienol (TCT) form of natural vitamin E is substantially more potent than the better known  $\alpha$ -tocopherol for its neuroprotective properties.<sup>3</sup> In several biological contexts the two major forms of vitamin E,  $\alpha$ -tocopherol and TCT, are known to exhibit contrasting functions.<sup>4</sup> In stroke, while TCT is protective,  $\alpha$ -tocopherol may

exacerbate microglial activation and worsen stroke outcomes.<sup>5</sup> Work from our laboratory has demonstrated protective effects of nanomolar TCT against stroke in small and large animals.<sup>6–9</sup> Recent work has shown that, in patients who have suffered a mini-stroke and are at a serious risk of a major stroke, TCT supplementation was beneficial. A higher incidence of aspirin resistance was observed in patients on aspirin and clopidogrel than in all the patients treated with aspirin alone and TCT. The frequency of aspirin resistance decreased in response to TCT supplementation.<sup>10</sup>

Multiple molecular mechanisms responsible for the potent neuroprotective effects of TCT have been reported in small-animal models of stroke.<sup>4,6,8,11–13</sup> The study of stroke in a large-animal model revealed a cerebrovascular function of TCT.<sup>9,14,15</sup> Fluoroscopy-guided angiography demonstrated that TCT protected against ischemic stroke by improving blood flow to the stroke-affected site.<sup>9</sup> The infarcted brain tissue core constitutes permanently damaged tissue secondary to a significantly lowered blood supply. The penumbra surrounding the core stroke-affected tissue is threatened by ischemia. However, it may be rescued by appropriate local perfusion pressures.<sup>16</sup> After stroke, high collateral blood flow may rescue the penumbra tissue from irreversible infarction. Under certain conditions, prompt reperfusion by restoring the blood flow can potentially save and restore normal cell function in the penumbra.<sup>17</sup> Acute stroke therapeutics aim to limit tissue damage occurring at the “penumbra” level and restore the functionality of the related brain tissue. Thus, re-establishment of the functional cerebral microvascular network is of critical significance to promote stroke recovery. Improving the functional recovery after ischemic stroke is crucial to increasing life expectancy and quality of life.<sup>18</sup> In this work, our effort to understand the molecular basis of the effect of TCT in improving blood supply to the stroke-affected site of the

Received 7 July 2022; accepted 31 December 2022;  
<https://doi.org/10.1016/j.omtn.2022.12.019>

**Correspondence:** Savita Khanna, PhD, Department of Surgery, Indiana Center for Regenerative Medicine and Engineering, Indiana University School of Medicine, Indianapolis, IN 46202, USA.

**E-mail:** [sjkhanna@iu.edu](mailto:sjkhanna@iu.edu)



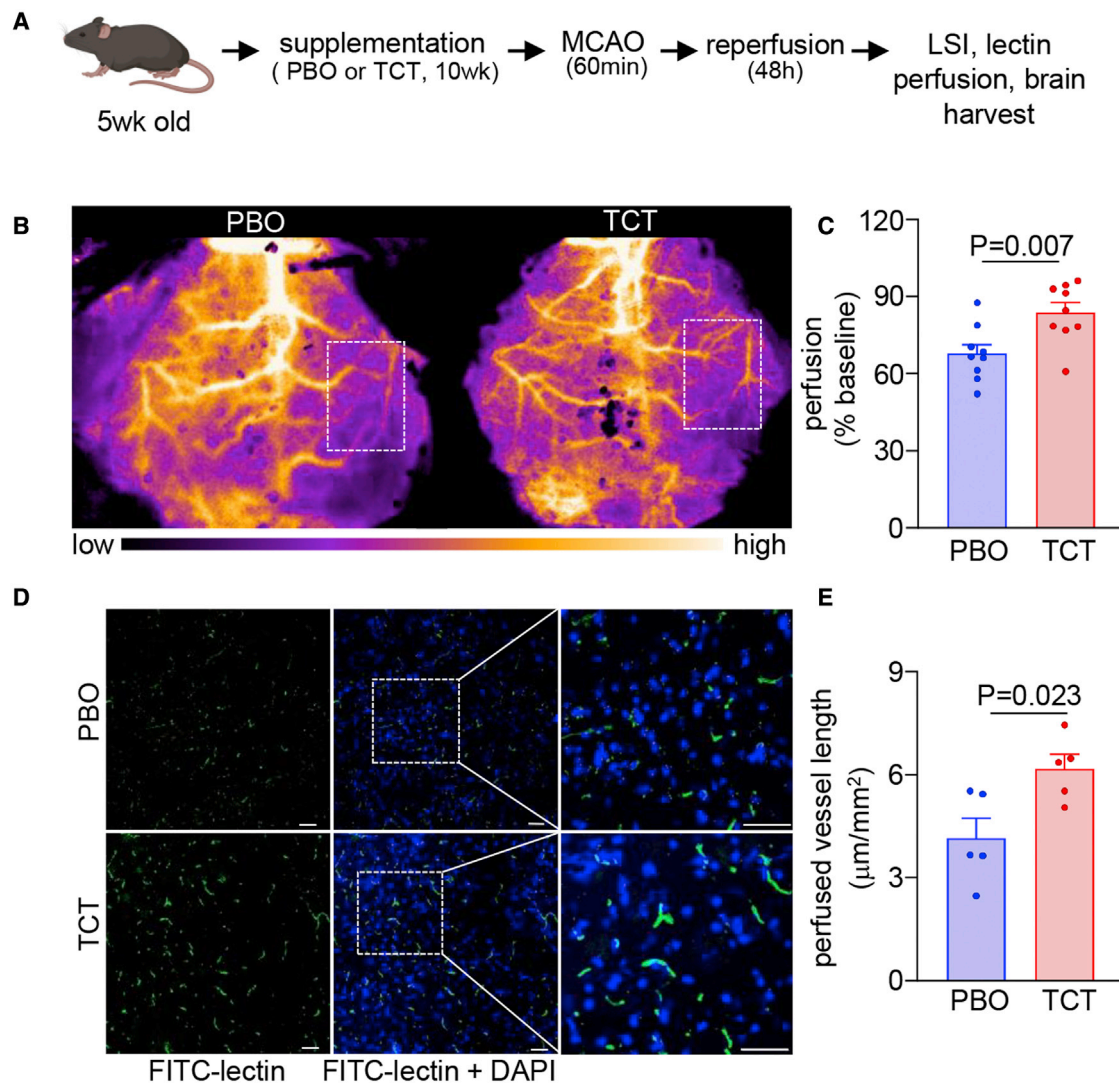


**Figure 1. TCT supplementation improved perfusion at the stroke-affected mouse brain site**

(A) Experimental timeline of TCT supplementation, MCAO, and brain harvest. C57BL/6 mice were supplemented with vitamin E-stripped corn oil (vehicle) placebo (PBO) or TCT (50 mg/kg bw) for 10 weeks before MCAO. (B) Real-time, noninvasive, cerebrovascular perfusion imaging of the dorsal surface of the stroke-affected brain was acquired in mice at 48 h of reperfusion using PeriScan PSI laser speckle flowmetry. (C) Perfusion quantification. TCT-supplemented mice had significantly higher perfusion in the stroke-affected brain site ( $n = 9$ ). (D and E) TCT treatment resulted in the detection of more patent vascular structures in the S1 cortex by FITC-lectin at 48 h after MCAO. After 48 h of post-MCAO reperfusion, FITC-conjugated lectin was injected directly into the left ventricle of the heart. Ten minutes after the lectin injection, the mice were euthanized, and brains were collected in OCT. (D) Representative fluorescence micrographs of stroke-affected S1 cortex from PBO and TCT mice. The inset images (indicated by white dashed lines) show a zoomed-in view of the selected region on the right. Scale bars, 50  $\mu\text{m}$ . (E) Quantification of lectin-perfused vessel length ( $\text{mm}^2$  area,  $n = 5$ ). Data are shown as mean  $\pm$  SEM.

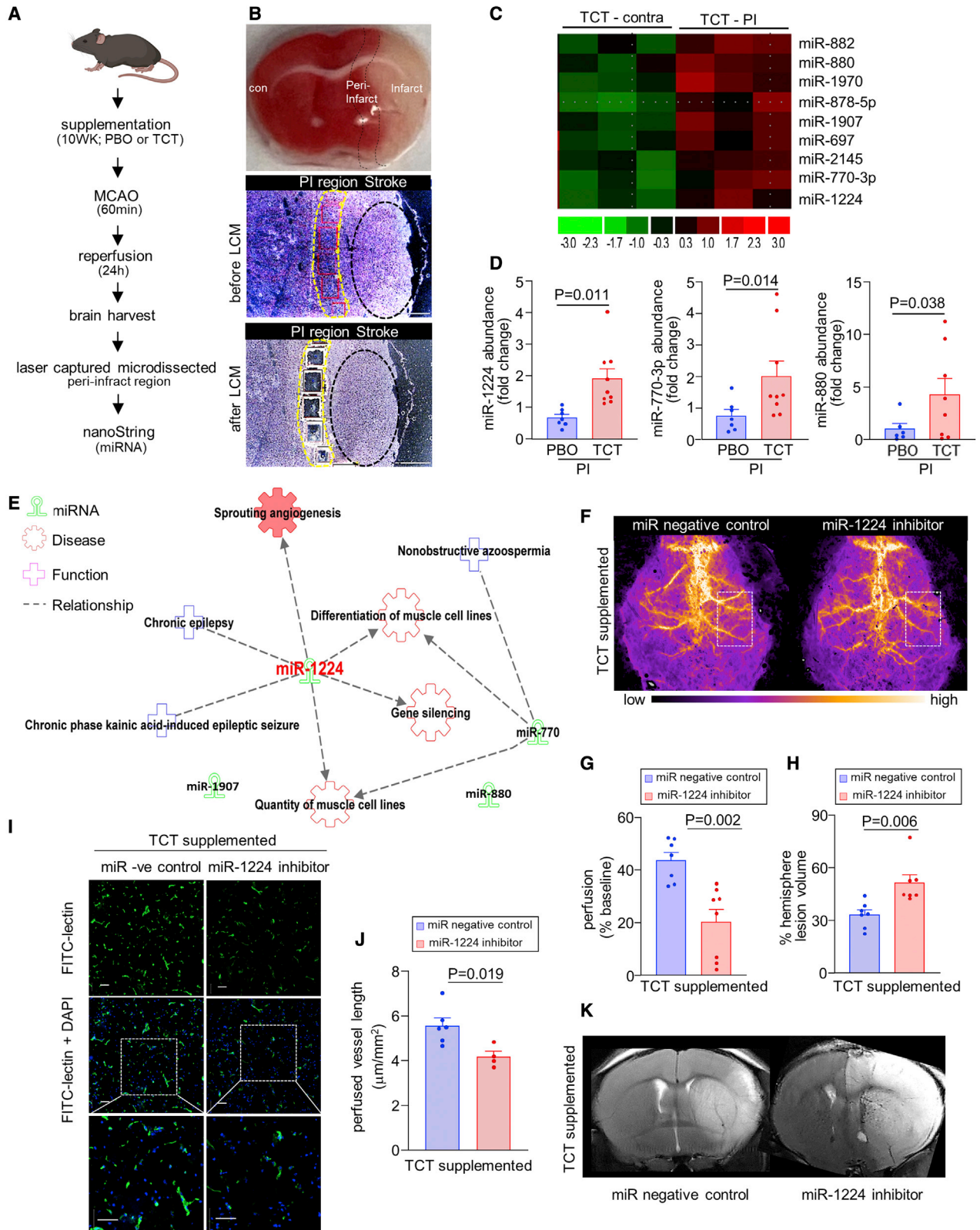
brain uncovered a mechanistic pathway heretofore unknown to regulate cerebrovascular perfusion.

## RESULTS

### TCT supplementation improved perfusion at the stroke-affected site by inducing miR-1224

Laser speckle imaging (LSI) analyses showed significantly higher cerebrovascular perfusion in the stroke-affected site of the brain at 48 h after

middle cerebral artery occlusion (MCAO) in TCT-supplemented mice compared with placebo (PBO)-supplemented mice (Figures 1A–1C). Endothelial binding of fluorescein isothiocyanate (FITC)-lectin revealed cerebrovascular structures in the stroke-affected brain tissue. TCT supplementation improved the abundance of vascular structures in the stroke-affected S1 cortex at the stroke-affected site (Figures 1D and 1E). No differences in perfusion were detected in the contralateral hemisphere between PBO- and TCT-supplemented mice (Figures S1A



(legend on next page)

and S1B). To understand the molecular basis of the effect of TCT on perfusion at the stroke site, the ipsilateral peri-infarct area and the corresponding contralateral area were laser-capture microdissected for expression profiling of microRNA (Figures 2A–2C). Differentially expressed miRNAs (Figures 2C and S3A) were identified. These differentially expressed miRNAs were validated by quantitative real-time PCR. miR-1224, miR-770, and miR-880 were significantly upregulated in response to TCT supplementation (Figures 2D and S3B). Ingenuity Pathway Analysis (IPA) (Figure 2E) of TCT-sensitive miRNAs revealed that miR-1224 was the only miRNA that was involved in sprouting angiogenesis (Figure S3C). miR-1224 was abundant in the brain microvascular endothelial cells (Figure S2G). IPA also linked other TCT-sensitive miRNAs to the hub miR-1224 in the context of angiogenic function (Figure 2E). Produced by intronic splicing, miR-1224 is a mammalian mirtron present in the last intron of the von Willebrand factor A domain-containing 5B2 (VWA5B2) gene.<sup>19</sup>

To examine the IPA-predicted significance of TCT-sensitive miR-1224 in cerebral perfusion, stroke experiments were repeated under conditions of miR-1224 knockdown. miR-1224 was knocked down using a lentiviral vector to deliver shRNA (LentimiRa-off-GFP or LentimiRa-off-mmu-miR-1224-5p,  $10^8$  IU/mL). Note that these experiments include injection of a viral vector into the stroke site of the brain, and therefore baseline values of any reading differ from settings not involving any viral gene delivery, which is known to cause mild inflammation in the affected tissue.<sup>20–22</sup> The viral vector was delivered to the stroke site of TCT-supplemented mice using stereotaxic injection (coordinates:  $-0.5$  mm posterior,  $+3.5$  mm lateral, and  $-2.0$  mm ventral to bregma). After 7 days of such lentiviral miR-1224 inhibitor delivery, the mice were subjected to MCAO, and cerebrovascular perfusion was evaluated using LSI and lectin perfusion. Lentiviral knockdown of miR-1224 was successfully achieved (Figure S3D). miR-1224 inhibition lowered stroke-site perfusion of TCT-supplemented mice (Figures 2F and 2G). Patent vascular structures were fewer, indicative of lower collateral blood flow (Figures 2I and 2J) in the stroke-affected brain site. In the context of previous studies that have reported on the beneficial effects of TCT supplementation

on stroke-induced brain injury,<sup>7–9</sup> it was noted that tissue injury of TCT-supplemented mice was worsened under conditions of miR-1224 knockdown (Figures 2H and 2K).

#### Proangiogenic miR-1224

Brain endothelial cells were studied to test possible angiogenic effects of miR-1224. Thus, Matrigel tube formation assay was performed using primary brain microvascular endothelial cells (pMBMECs) (Figure 3) or bEnd.3 cells (Figure S4). pMBMECs were transfected with control mimic or miR-1224 mimic for 72 h. Delivery of mimic was effective in significantly augmenting miR-1224 levels (Figure 3B). These cells showed significantly higher angiogenic properties (Figure 3A). Delivery of miR-1224 bolstered Matrigel tube formation. Total tube length (Figure 3C), number of nodes (Figure 3D), number of junctions (Figure 3E), and number of meshes (Figure 3F) were increased in cells rich in miR-1224. Consistent proangiogenic effects of miR-1224 were noted in bEnd.3 cells (Figure S4).

#### Functional significance of miR-1224 in stroke *in vivo*

To understand the functional significance of miR-1224 in stroke, control mimic (pLenti-III-mir-GFP control miRNA) or miR-1224 mimic (pLenti-III-mmu-miR-1224 ( $10^8$  IU/mL)) was stereotaxically delivered to the S1 cortex (Figure 4A) 72 h before stroke surgery. The microRNA delivery significantly elevated brain tissue miR-1224 levels (Figure S5). After 72 h of miR-1224 mimic delivery, the mice were subjected to MCAO. LSI analysis revealed significant increase in blood perfusion levels in miR-1224 mimic-delivered stroke-affected brain (Figures 4B and 4C). A significant increase in patent vascular structures in the stroke-affected site of the brain was noted as detected by FITC-lectin perfusion (Figures 4D and 4E). MRI analysis of stroke-induced brain tissue injury demonstrated a protective effect of the miR-1224 mimic (Figures 4F and 4G). The study of post-stroke functional outcome was conducted by assessment of spontaneous locomotor activity of the stroke-affected mice at baseline and 48 h post-stroke. In this open-field test, the miR-1224 mimic markedly improved outcomes (Figures 4H and 4I). In response to miR-1224 mimic delivery, stroke-affected mice moved faster, farther, and for a longer duration.

### Figure 2. miR-1224 is responsible for the beneficial effects of TCT supplementation on post-stroke cerebrovascular perfusion of the stroke site as well as on stroke lesion size

(A) Timeline of TCT supplementation, MCAO, and brain harvest. C57BL/6 mice were supplemented with PBO (vehicle) or TCT (50 mg/kg bw) for 10 weeks before MCAO. (B) After 24 h of stroke, coronal slices of brain tissue were collected using a mouse brain matrix. OCT-embedded slices were subsequently cut in  $12\text{-}\mu\text{m}$ -thick sections. Matched areas ( $2 \times 10^6 \mu\text{m}^2$ ) of the ipsilateral peri-infarct area (PI) and contralateral peri-infarct (contra) area were laser captured for the analysis of microRNA expression. (C) Heatmap visualization of differentially expressed miRNAs in TCT-supplemented murine brain using NanoString nCounter miRNA expression assays. The color code in the heatmap is linear, with green representing the lowest and red representing the highest expression. (D) Validation of TCT-sensitive mmu-miRNA using quantitative real-time PCR shows that miR-1224, miR-770-3p, and miR-880 were upregulated in TCT-supplemented post-stroke murine brain ( $n = 7$  and  $9$ ). The miRNA expression level was normalized to that of U6 snRNA. (E) Biofunction analysis of differentially expressed TCT-sensitive microRNAs using the Ingenuity Pathway Analysis (IPA) tool. miR-1224 was the only miR that was called as being involved in angiogenesis. For knockdown of miR-1224 in TCT-supplemented mice, LentimiRa-off-GFP or LentimiRa-off-mmu-miR-1224-5p ( $10^8$  IU/mL) was delivered to the cortex of mice using stereotaxic injection. After 7 days of such gene silencing, mice were subjected to MCAO. Real-time, noninvasive, cerebrovascular perfusion imaging of the dorsal surface of the brain was acquired in mice during occlusion and at 48 h of perfusion using PeriScan PSI laser speckle flowmetry. (F) Representative tracings for perfusion assessment. (G) Perfusion quantification. miR-1224 inhibitor significantly lowered perfusion in the stroke-affected brain site ( $n = 7$  and  $6$ ). (H–K) In TCT-supplemented mice, miR-1224 inhibition downregulated stroke-site perfusion as well as the abundance of patent vascular structures in S1 cortex as detected by FITC-lectin perfusion (I and J,  $n = 6$  and  $4$ ). The inset images (indicated by white dashed lines) show a zoomed-in view of the selected region on the bottom. Scale bars,  $50 \mu\text{m}$ . Delivery of miR-1224 inhibitor worsened the stroke-induced brain injury in TCT-supplemented mice. Representative 9.4 T MRI (48 h) images (K) and lesion area quantitation (H,  $n = 7$  and  $7$ ). Data are shown as mean  $\pm$  SEM.

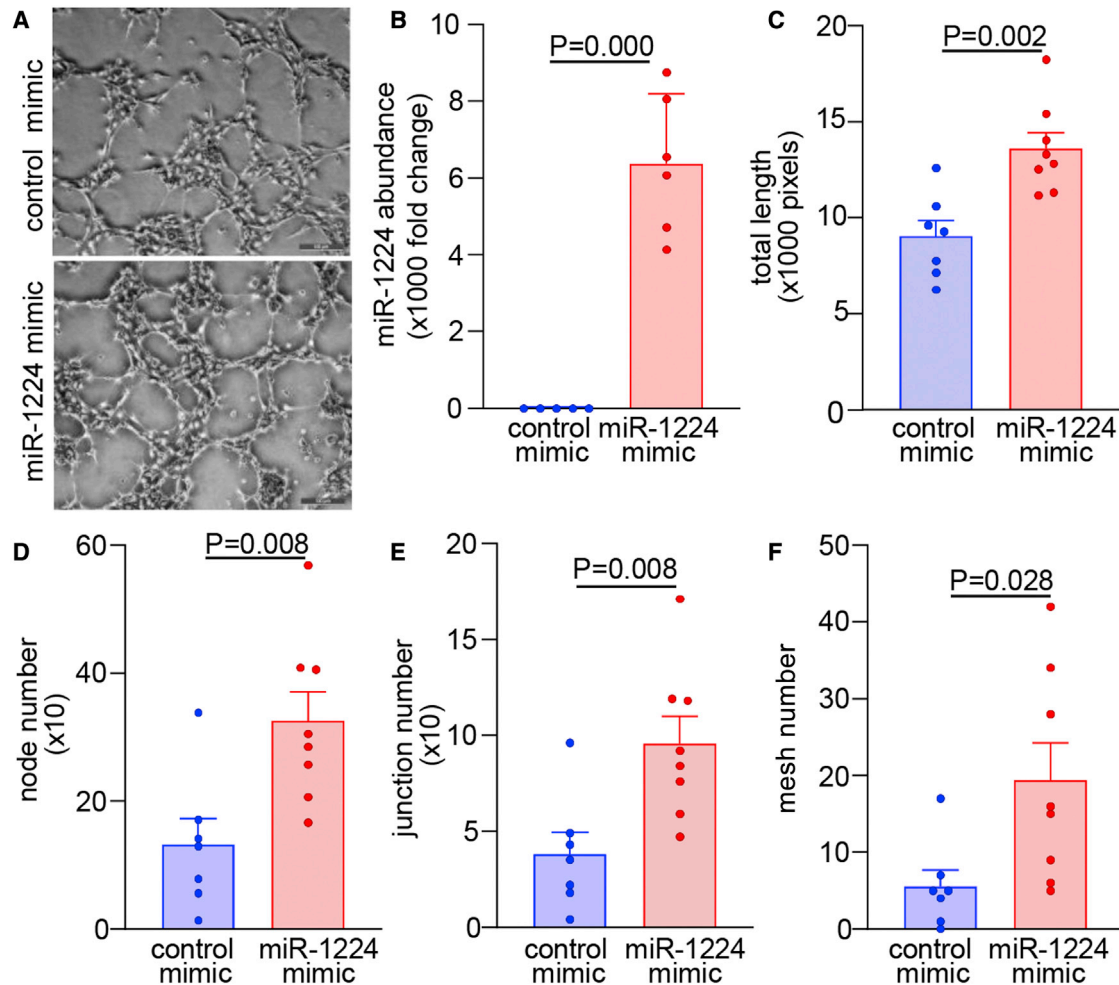


**Figure 3. miR-1224 exhibited proangiogenic effects in mouse primary brain microvascular endothelial cells**

Matrigel tube formation was visualized by phase-contrast microscopy at 18–24 h in control mimic- or miR-1224 mimic-transfected cells. pMBMECs transfected with control mimic or miR-1224 mimic were plated on Matrigel 72 h after transfection. (A) Representative images of tube formation in control- and miR-1224 mimic-transfected pMBMECs. Scale bars, 100  $\mu$ m. (B) Real-time PCR analysis of miR-1224 after transfection of miR-1224 mimic (n = 5 and 6). (C–F) Angiogenic parameters were quantified (n = 7 and 8) using ImageJ software and the Angiogenesis Analyzer plug-in tool. (C) Total tube length, (D) number of nodes, (E) number of junctions, and (F) number of meshes. Data are shown as mean  $\pm$  SEM.

#### Anti-angiogenic *Serpine1* is a target of miR-1224

With the objective of understanding the molecular mechanisms responsible for the proangiogenic effects of miR-1224, murine brain microvascular endothelial cells were studied. The simultaneous screening of 53 murine angiogenesis-related proteins identified potential miR-1224 targets (Figure 5A). Histogram protein expression profiles were generated for such targets (Figure S6A). *Serpine1* emerged as a candidate target of miR-1224. To test whether *Serpine1* is indeed a target of miR-1224, standard target validation tests were performed. Delivery of miR-1224 to brain endothelial cells lowered SERPINE1 expression (Figures 5B and 5C). Next, we performed *in silico* studies to test whether *Serpine1* can be a potential target of miR-1224 as predicted by the miRWalk, TargetScan, PicTar, miRDB, miRanda, RNA22, and PITA algorithms.<sup>23–27</sup> *In silico* analyses of

the SERPINE1 3' UTR revealed binding sites for miR-1224 (Figures 5D and S6B). To determine if *Serpine1* is targeted by miR-1224, a reporter assay was performed on a construct with the luciferase gene with the 3' UTR of SERPINE1. Elevated levels of miR-1224, via mimic delivery in bEnd.3 cells with the wild-type SERPINE1 3' UTR, suppressed luciferase activity (Figure 5E). This silencing effect was not observed following mutation of the miR-1224 binding site on the 3' UTR of SERPINE1 (Figure 5E). These findings demonstrate miR-1224-mediated silencing of *Serpine1*. Taken together, it is thus established that *Serpine1* is a target of miR-1224 in brain endothelial cells.

Downregulation of *Serpine1* augmented the angiogenic response of the miR-1224 mimic in the murine brain endothelial cells. To

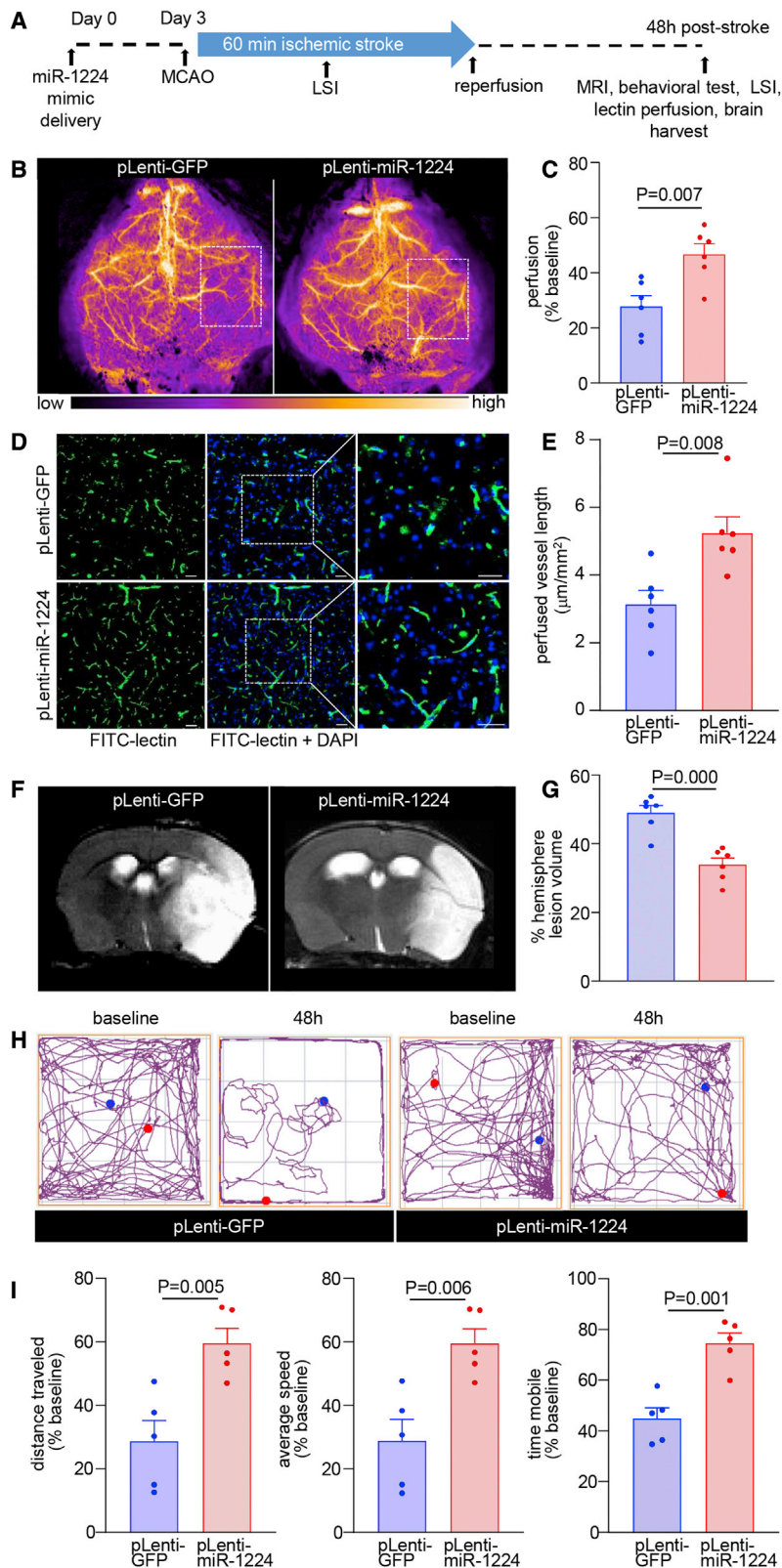


**Figure 4. Delivery of miR-1224 mimic to the brain improved cerebrovascular blood flow at the stroke-affected site and protected against stroke**

(A) Timeline of miR-1224 delivery, MCAO, LSI, MRI, and brain harvest. Targeted delivery of pLenti-III-mir-GFP control miRNA (pLenti-GFP) or pLenti-III-mmu-miR-1224 (pLenti-miR-1224,  $10^8$  IU/mL) to the MCA-supplied S1 cortex of C57BL/6 mice was achieved by stereotaxic injection using a Hamilton syringe connected to a nano-injector. After 72 h of such gene delivery, the mice were subjected to MCAO. Real-time, noninvasive, cerebrovascular perfusion imaging of the dorsal surface of the brain was acquired in the mice during occlusion and at 48 h of perfusion using PeriScan PSI laser speckle flowmetry. (B) Laser speckle images collected 48 h post-stroke. (C) Quantification of perfusion as evident in (B);  $n = 6$ . (D) miR-1224 delivery improved FITC-lectin perfusion to S1 cortex at the stroke-affected site 48 h post-stroke. The inset images (indicated by white dashed lines) show a zoomed-in view of the selected region on the right. Scale bars,  $50 \mu\text{m}$ . (E) Quantification of lectin-perfused vessel length ( $\mu\text{m}^2$  area,  $n = 6$ ). (F) Representative 9.4 T MRI (48 h post-stroke) images and (G) lesion area quantitation ( $n = 6$ ). (H) Representative track plots from baseline and 48 h post-stroke. Tracks start at blue dots and end at red dots. (I) Delivery of miR-1224 mimic significantly improved distance traveled, mean speed, and time mobile ( $n = 5$ ) compared with control. Data are shown as mean  $\pm$  SEM.

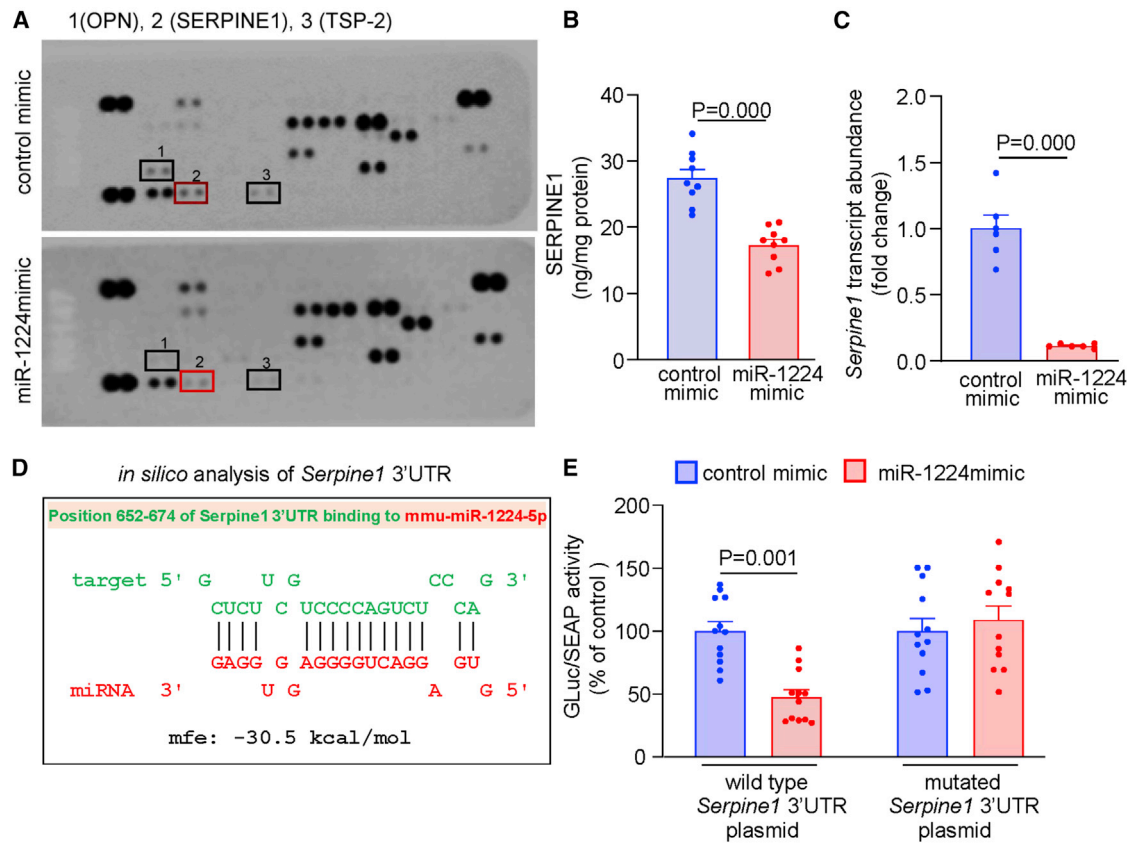


**Figure 5. *Serpine1* is a target of miR-1224**

(A) Angiogenic protein array showing the difference in control mimic- and miR-1224 mimic-transfected bEnd.3 cells. The Proteome Profiler Mouse Angiogenesis Array Kit (cat. no. ARY015) was used to simultaneously assess the relative levels of 53 mouse angiogenesis-related proteins. (B) SERPINE1 protein (n = 9) and (C) *Serpine1* transcript abundance in miR-1224 mimic-delivered cells (n = 6). (D) Binding site to mouse transcript ENSMUST0000041388-3' UTR position 652–674 to miR-1224-5p (MIMAT0005460); binding energy –30.5 kcal/mol. Proposed binding sites for miR-1224 were identified in the SERPINE1 3' UTR that was inserted into the *Gaussia* luciferase plasmid vector (wild type). The pEZX-MT05 vector also contains the secreted *Gaussia* luciferase (GLuc) open reading frame, driven by the SV40 promoter, as a reporter of the 3' UTR expression, and a secreted alkaline phosphatase (SEAP) reporter, driven by a CMV promoter, as an internal control. (E) Quantification of luciferase reporter assay (n = 12) of wild-type and mutated versions of the miR-1224 binding site on the SERPINE1 3' UTR. GLuc activity and alkaline phosphatase activity were assayed after 48 h of transfection using GeneCopoeia's Secrete-Pair dual luminescence assay kit. Percentage change in GLuc activity was calculated after normalizing to alkaline phosphatase activity. Data are shown as mean  $\pm$  SEM.

specifically link lower *Serpine1* to angiogenic responses, specific SERPINE1 siRNA was delivered to brain endothelial cells (Figures 6A–6F). In the interest of rigor, an additional small-molecule inhibitor of SERPINE1, TM5441,<sup>28</sup> was also tested (Figures 6G–6K). siRNA-dependent knockdown of SERPINE1 was successful (Figures 6B and S7A). Matrigel tube formation assay run with pMBMECs (Figure 6) or bEnd.3 cells (Figure S7) established that lowering of *Serpine1* bolstered angiogenic outcomes (Figures 6A–6F and S7B–S7F). *Serpine1* inhibition resulted in increased total tube length (Figures 6C, 6H, S7C, and S7H), number of nodes (Figures 6D, 6I, S7D, and S7I), number of junctions (Figures 6E, 6J, S7E, and S7J), and number of meshes (Figures 6F, 6K, S7F, and S7K).

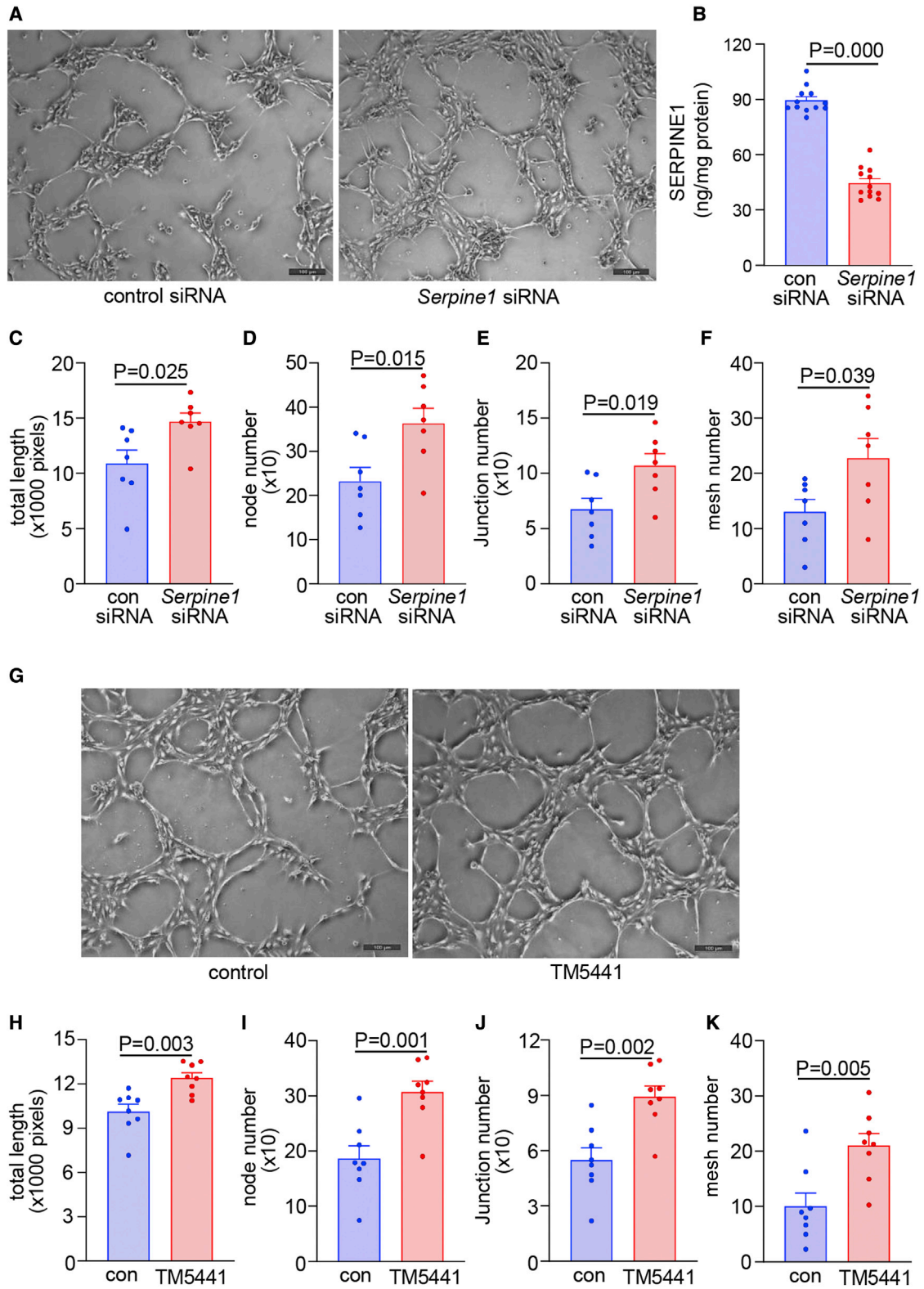
#### SERPINE1 inhibition improved stroke outcomes *in vivo*

The *Serpine1* gene encodes the protein plasminogen activator inhibitor 1 (PAI-1). TM5441 inhibits PAI-1.<sup>28–30</sup> The experimental design to test the effects of inhibition of SERPINE1 on stroke outcomes is de-

picted in Figure 7A. The inhibition of SERPINE1 increased cerebrovascular blood flow at the stroke-affected site and protected against stroke. LSI analysis revealed significant increase in blood perfusion levels in the stroke-affected brain of the TM5441-treated group (Figures 7B and 7C). Significantly increased FITC-lectin perfusion in vessels was also observed following such treatment (Figures 7D and 7E). MRI analyses, 48 h after MCAO, revealed that TM5441 protected against stroke-induced brain lesion (Figures 7F and 7G). Spontaneous locomotor activity assessed at baseline and 48 h post-stroke with an open-field test demonstrated marked improvement in TM5441-treated mice (Figures 7H and 7I). Mice moved faster, farther, and for a longer duration compared with controls.

#### DISCUSSION

Following stroke, injury to the brain tissue is exacerbated by a fibrin clot.<sup>31–33</sup> Physiological defense against such threat is afforded by urokinase plasminogen activator (uPA) and tissue-type plasminogen



(legend on next page)

activator (tPA). PAI-1 inhibits these defense systems in the context of stroke. Thus, downregulation of PAI-1 in such context is desirable. PAI-1, also known as endothelial plasminogen activator inhibitor or Serpine1, is a human protein and, in humans, is encoded by the *SERPINE1* gene. *SERPINE1* belongs to the serine proteinase inhibitor (serpin) superfamily. Over a decade ago *SERPINE1* was recognized as a stroke-risk gene.<sup>34</sup> In MCAO-based experimental stroke, murine *Serpine1* gene expression is induced in both males and females.<sup>35</sup> PAI-1 gene deficiency attenuates ischemic brain injury following experimental stroke.<sup>36</sup> Downregulation of inducible PAI-1 expression also improves recovery after acute ischemic stroke.<sup>37</sup> A recent work investigating the protective effect of dauricine against murine MCAO-based stroke identified inhibition of *SERPINE1* by dauricine as its primary mechanism of action. A chemotactic effect of *SERPINE1* responsible for exacerbation of stroke-related neuroinflammation by enhanced recruitment of peripheral neutrophil has been reported.<sup>38</sup> The study of established biomarkers of death from ischemic stroke versus stroke survival revealed *SERPINE1* as part of a highly connective protein-protein interaction network associated with death caused by ischemic stroke.<sup>39</sup> In patients with pseudoxanthoma elasticum, a rare autosomal recessive disorder caused by pathogenic variants in the *ABCC6* gene, a 4G/4G *SERPINE1* genotype contributes to an added risk for developing ischemic stroke.<sup>40</sup> This work, the primary objective of which was to identify the molecular mechanism of action of a lesser-known isoprenoid form of natural vitamin E, TCT, recognized inhibition of *Serpine1* as a major mechanism of action. What is strikingly interesting about this finding is that *Serpine1* is causatively connected to the negative regulation of perfusion of the affected brain site following stroke. This constitutes the first evidence assigning cerebrovascular function to *Serpine1*. The significance of this observation is heightened by reports establishing that, in the context of tumor biology, Serpine1 or PAI-1 displays provascular functions.<sup>41–44</sup>

Elevated expression of *SERPINE1* has been associated with several cancers.<sup>45</sup> Thus, mechanisms underlying post-transcriptional silencing of this gene have drawn much interest. The study of a number of healthy and diseased cells shows that the significance of *SERPINE1* depends on the cell compartment in question. Earlier studies reporting on this gene in human keratinocytes assigned it a wound repair function.<sup>46,47</sup> Yet, in cancer cells, it contributes to cell proliferation, migration, and metastases.<sup>45</sup> In tumors, extravascular fibrin provides a scaffolding function to harbor and support endothelial cell growth and motility as required for angiogenesis. The study of mice with targeted disruption of *Tgfb2* in the endothelium demon-

strated that TGF- $\beta$  signaling-dependent induction of *Serpine1* is necessary for tumor angiogenesis. Post-transcriptional silencing of *Serpine1* by miR-30c inhibited tumor angiogenesis.<sup>48</sup> Furthermore, independent work has demonstrated that members of the miR-30 family of miRNAs target the *Serpine1* gene and regulate endothelial cell morphogenesis.<sup>49–51</sup> miR-30b downregulation is associated with high-serum PAI-1 under conditions of neonatal hypoxic-ischemic encephalopathy.<sup>52</sup> In human endothelial cells, miR-421 and miR-30c silence *SERPINE1* gene expression.<sup>51</sup> In the endothelial cell compartment, the detrimental effects of PAI-1 have multiple mechanisms of action. In the kidney, PAI-1 causes glomerular endothelial senescence, which contributes to age-related kidney disease.<sup>53</sup> Elevated Serpine1 is associated with metabolic diseases and also with age-related increase in the occurrence of thrombosis.<sup>54–56</sup> Senescent cells characteristically express Serpine1 as part of the senescence-associated secretory phenotype.<sup>57</sup> In sickle-cell disease, high levels of PAI-1 may cause endothelial dysfunction and exacerbate disease severity.<sup>58</sup> High endothelial PAI-1 may contribute to prothrombotic events in patients with COVID-19.<sup>59</sup> Bacterial products such as lipopolysaccharides potently induce PAI-1 by downregulating miR-30c.<sup>60</sup> In the life-threatening condition of cytokine release syndrome, as well as in those suffering from COVID-19, management of high levels of PAI-1 provided symptomatic relief. IL-6 induced PAI-1 in vascular endothelial cells, causing endotheliopathy in those affected by cytokine release syndrome.<sup>61</sup>

Bone marrow mesenchymal stem cells have drawn interest as a therapeutic tool to treat many pathologies, including nontraumatic osteonecrosis of the femoral head. A recent work raises the concern that miR cargo of exosomes derived from these stem cells may upregulate PAI-1 in vascular cells, which is known to be positively associated with this disabling orthopedic disease.<sup>62</sup> In human umbilical vein endothelial cells, docosahexaenoic acid, which is known to be a healthy dietary factor, induced miR-3691-5p to post-transcriptionally silence *SERPINE1*.<sup>63</sup> In the setting of hepatopulmonary syndrome, PAI-1 in pulmonary microvascular endothelial cells is a direct target of miR-145-5p.<sup>64</sup> A separate study on human pulmonary microvascular endothelial cells reported on targeting of PAI-1 by miR-30c and miR-301a.<sup>65</sup> In human aortic endothelial cells, PAI-1 silencing by miR-19b and miR30c provided relief against atherosclerosis.<sup>66</sup> In human coronary artery endothelial cells, miR-17 downregulated PAI-1 and helped manage hypertension.<sup>66</sup> The deleterious effects of human microvascular endothelial cell PAI-1 on lung fibrosis related to sickle-cell disease have been managed by miR-301a/miR-454.<sup>67</sup> Long noncoding RNAs (lncRNAs) outcompete endogenous RNAs

#### Figure 6. Downregulation of *Serpine1* induced angiogenic response in mouse primary brain microvascular endothelial cells

Matrigel tube formation was visualized by phase-contrast microscopy at 18–24 h in control or *SERPINE1* siRNA-transfected cells. pMBMECs transfected with nontargeting siRNA (control siRNA) or *SERPINE1* siRNA were plated on Matrigel 72 h following transfection. (A) Tube formation in control and *SERPINE1* siRNA-transfected pMBMECs. Scale bars, 100  $\mu$ m. (B) *SERPINE1* protein (ELISA) after transfection of *SERPINE1* siRNA (n = 12). Standard angiogenic parameters were quantified (n = 7) using ImageJ and the Angiogenesis Analyzer plug-in tool. (C) Total tube length, (D) number of nodes, (E) number of junctions, and (F) number of meshes. Data shown as mean  $\pm$  SEM. (G–K) Alternative studies were conducted with the *SERPINE1* inhibitor TM5441. (G) Tube formation in control and TM5441 (10  $\mu$ M, 24 h)-treated pMBMECs. Scale bars, 100  $\mu$ m. Angiogenic parameters were quantified (n = 8) using ImageJ and the Angiogenesis Analyzer plug-in tool. (H) Total tube length, (I) number of nodes, (J) number of junctions, and (K) number of meshes. Data are shown as mean  $\pm$  SEM.

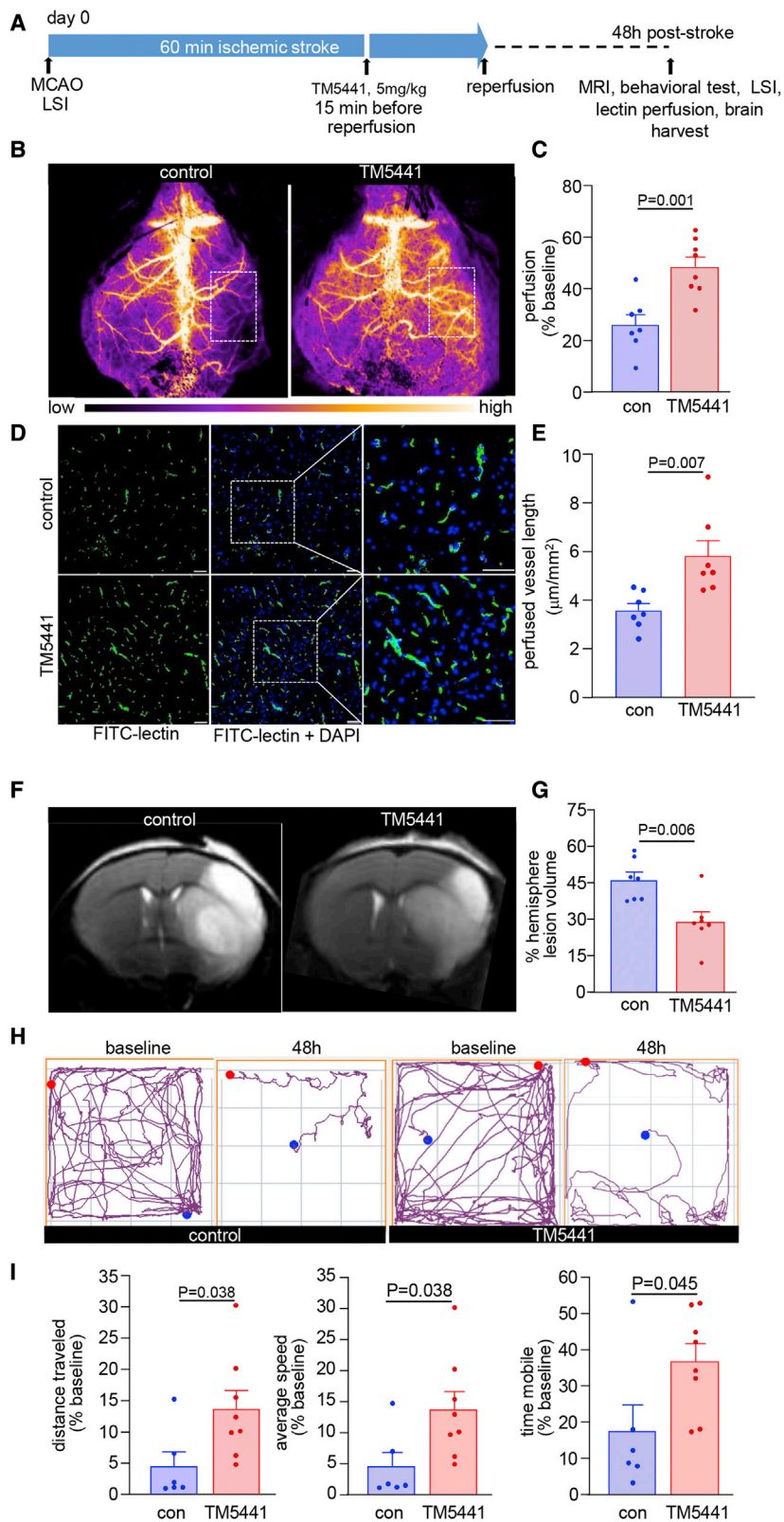


**Figure 7. Small-molecule SERPINE1 inhibition increased cerebrovascular blood flow at the stroke-affected site and protected against stroke**

(A) Timeline of TM5441 treatment, MCAO, LSI, MRI, and brain harvest. (B) Real-time, noninvasive, cerebrovascular perfusion images of the dorsal surface of the brain were acquired in mice during occlusion and at 48 h post-stroke. (C) Perfusion quantification in TM5441-treated mice showed significantly higher perfusion in stroke-affected brain (n = 7 and 8). The SERPINE1 inhibitor TM5441 improved FITC-lectin perfusion to the S1 cortex at the stroke-affected site at 48 h post-stroke. (D) Fluorescence micrographs of stroke-affected S1 cortex of control and TM5441-treated mice. The inset images (indicated by white dashed lines) show a zoomed-in view of the selected region on the right. Scale bars, 50  $\mu\text{m}$ . (E) Quantification of lectin-perfused vessel length ( $\mu\text{m}^2$  area, n = 7). (F) Representative 9.4 T MRI (48 h post-stroke) images and (G) percentage hemisphere lesion volume calculated based on T2-weighted MRI at 48 h post-stroke (n = 7). (H) Representative mobility track plots from baseline and 48 h post-stroke of control or TM5441-treated mice. Tracks start at blue dots and end at red dots. (I) TM5441 treatment significantly improved 48 h post-stroke distance traveled, mean speed, and time mobile (n = 6 and 8) compared with control. Data are shown as mean  $\pm$  SEM.

to change the expression levels and downstream function of genes. In gastric cancer, the lncRNA NKX2-1-AS1 promoted tumor progression and angiogenesis by upregulating SERPINE1 expression and activating VEGFR-2 signaling.<sup>44</sup>

Heretofore, endothelial miR-1224 has been reported in a few publications, none of which involves the brain. This work presents the maiden report that miR-1224 exists in the brain in a way that is inducible by the TCT form of dietary natural vitamin E. A substantial body of literature supports the potent neuroprotective and stroke-therapeutic functions of TCT.<sup>7-10,68</sup> More recent work involving angiography of the canine stroke-affected brain highlights the involvement of TCT in improving cerebrovascular perfusion of the stroke-affected site.<sup>9,15</sup> This work reveals *Serpine1* as an angiostatic factor in the stroke-affected brain. Such finding, although opposing the vast literature on the proangiogenic effects of *Serpine1* in tumor biology, is consistent with observations of *Serpine* reported from scenarios not involving the central nervous system or cancer (Figure S8). In human umbilical vein endothelial cells, PAI-1 binds to eNOS to inhibit eNOS function, which is known to be necessary for angiogenesis.<sup>69</sup> This, unlike observations discussed above in the tumor biology setting, assigns an angiostatic function to PAI-1.<sup>69,70</sup> Both eNOS and tPA are negatively regulated by PAI-1. Thus, low PAI-1 conditions would favor optimal and augment functioning of eNOS and tPA simultaneously. Such conditions, also achieved by statin treatment, are known to improve ischemic stroke outcomes.<sup>71</sup> The angiostatic effects of PAI-1 have been evident in the setting of myocardial infarction.<sup>72</sup>

The significance of the findings of this work should account for the inherent limitations and strengths. The favorable effects of TCT against stroke, as reported in this work, are specifically relevant to the prophylactic use of TCT. TCT is generally recognized as safe by the US FDA (GRAS no. 307). It may therefore be taken as a dietary supplement or food component. Long-term intake of TCT is known to enrich the lipophilic tissue, followed by sustained slow release to the circulation. Thus, in a prophylactic setting, this approach is likely to be beneficial as reported in a recent clinical study on patients who had suffered from mini-stroke and were therefore at a high risk of a major stroke.<sup>10</sup> On the use of TM5441 and miR-1224 mimic/inhibitors, please note that these were used as research reagents to test a mechanistic hypothesis. Extensive safety studies would be needed before these can be considered for use as therapeutic drugs.

Direct targeting of *Serpine1* by miR-1224 can improve perfusion of the stroke-affected brain. This addition to the larger landscape of the molecular basis of TCT protection against stroke is substantial because of the recently reported beneficial effects of dietary TCT supplementation on a cohort of 150 patients who had already suffered a mini-stroke and were therefore at a high risk for stroke.<sup>10</sup> Furthermore, because of the known neurodegenerative properties of fibrin clots,<sup>31-33</sup> the findings of this study provide the first intersection of TCT-sensitive mechanistic pathways that may be directly related to neuroprotective as well as provascular functions of natural vitamin E TCT in the context of ischemic stroke.

## MATERIALS AND METHODS

### Animal experiments

Male C57BL/6 mice were purchased from The Jackson Laboratory. All animal studies were performed in accordance with protocols approved by the Laboratory Animal Resource Center of Indiana University. Mice were maintained under standard conditions at 22°C ± 2°C with 12 h light/dark cycles and access to food and water *ad libitum*. No statistical methods were used to pre-determine the sample size. Power analysis was not necessary for this study. The animals were tagged and grouped randomly using a computer-based algorithm ([www.random.org](http://www.random.org)). For supplementation studies, mice were randomly divided into two groups, control and supplemented. The control group (PBO; vitamin-E-stripped corn oil) or test group (TCT; TCT-rich fraction of palm oil, 50 mg/kg body weight, ExcelVite, Malaysia) was orally gavaged for 10 weeks as described previously.<sup>6-8</sup>

### Gene delivery to the brain

To overexpress miR-1224 in mouse brain, pLenti-III-miR-GFP or pLenti-III-mmu-miR-1224-5p, miR-1224 lentiviral delivery to the male mouse brain cortex using stereotaxic injection (8 µL of 1.0 × 10<sup>8</sup> IU/mL; Applied Biological Materials, Richmond, BC, Canada) was done as described previously.<sup>6,73-75</sup> MCAO was performed to cause stroke in these mice 3 days after pLenti-III-mmu delivery. To achieve miR-1224 knockdown, LentimiRa-off-GFP or LentimiRa-off-mmu-miR-1224-5p was delivered as above to the brain cortex. MCAO was performed in mice 7 days after LentimiRa-off-mmu delivery.

### Small-molecule SERPINE1 inhibitor treatment

*Serpine1* is a serine (or cysteine) peptidase inhibitor (Gene ID: 18787), also known as PAI-1. Mice were treated with the small-molecule SERPINE1 inhibitor TM5441 (R&D Systems, Minneapolis, MN). TM5441 (5-chloro-2-[[2-[2-[[3-(3-furanyl)phenyl]amino]-2-oxoethoxy]acetyl]amino]benzoic acid sodium salt) was dissolved in DMSO, stored at -20°C, and diluted in saline before use. TM5441 (5 mg/kg) was administered by an intravenous (i.v.) injection 15 min before post-MCAO reperfusion. Control mice group received DMSO diluted in saline.

### MCAO experimental murine stroke

Transient focal cerebral ischemia was induced by MCAO as previously described.<sup>6,8,73-77</sup> Briefly, mice were anesthetized by inhaling isoflurane, and 6-0 nylon monofilament was inserted into the internal carotid artery via the external carotid artery. Next, the filament tip was positioned for occlusion at a distance of 6 mm beyond the internal carotid artery-pterygopalatine artery bifurcation. Once the filament was secured, the incision was sutured, and the occlusion was verified by LSI. Mice were allowed to recover from anesthesia in their cage. After 60 min of occlusion, the animal was briefly re-anesthetized, and reperfusion was initiated by withdrawal of the filament from MCA. Following stroke induction, subcutaneous injections of warmed saline were given to mice demonstrating signs of

dehydration, and hydrogel was provided to mice in addition to standard pellet food and water to promote nutrition uptake.<sup>76</sup> In total, 125 mice were used for all experiments. A total of 24 mice were excluded due to no stroke, hemorrhage, subcortical stroke, or death.

#### Laser speckle imaging

Mice were anesthetized and placed on a warm plate maintained at 37°C. After respiration was stabilized, perfusion recordings were performed using a PeriCam PSI Z system or PeriCam LSI HR system (Perimed, Sweden) per the manufacturer's instructions. Briefly, a 785 nm laser was used to illuminate the surface of the skull and the scattered light was recorded using a 2,048 × 2,048 (PSI Z system) or 752 × 580 (LSI HR system) pixel-resolution camera at a working distance of 10–12 cm and a maximum frame rate of 113 fps. Blood perfusion was calculated by analyzing the variations in the speckle pattern. From the real-time perfusion graphs, time-of-interest (TOI) was chosen to include lower peaks only to exclude respiratory motion-related artifacts. Average perfusion was calculated by using PimSoft v.1.5 software (Perimed, Sweden).

#### Magnetic resonance imaging and infarct volume determination

For infarct volume determination, T2-weighted imaging was performed on stroke-affected mice using a horizontal-bore 9.4 T Biospec pre-clinical MRI system (Bruker BioSpin MRI, Germany) as described previously.<sup>6,73–75</sup> For stroke volume calculations, raw MRI images were converted to digital imaging and communications in medicine (DICOM) format and read into ImageJ software (NIH). After matched contrast enhancement of images in ImageJ, digital planimetry was performed by a masked observer to delineate the infarct area in each coronal brain slice. Infarct areas from brain slices were summed, multiplied by slice thickness, and corrected for edema-induced swelling as previously described, to determine infarct volume.<sup>6,73,75</sup>

#### Open-field test

Spontaneous sensorimotor activity was assessed at baseline (pre-MCAO) and 48 h after stroke as described previously.<sup>6,73,75,76</sup> In brief, mice were placed in the center of a 1 × 1 m open field and allowed to freely move for 5 min while being recorded by an overhead camera using ANY-maze video tracking software (v.4.5; Stoelting, Wood Dale, IL). The system software calculated distance, mean speed, and time mobile for baseline and 48 h post-stroke time points.

#### Lectin perfusion of patent cerebrovascular structures

After 48 h of stroke, lectin perfusion was performed as described previously.<sup>78</sup> In brief, mice were deeply anesthetized using isoflurane, the thoracic cavity was opened, and 100 µg of FITC-conjugated tomato lectin (Sigma Aldrich; L0401) in 100 µL volume was injected directly into the left ventricle of the heart. Ten minutes after the lectin injection, the mice were euthanized, and brain tissue was sliced coronally using a brain matrix (Ted Pella, Redding, CA) and embedded in optimal cutting temperature compound (OCT) and cryosectioned at 10 µm thickness. Tissue sections were fixed with acetone. DAPI was used to stain the nucleus using Invitrogen ProLong Gold Antifade

mounting medium. The slides were scanned using Zeiss Axio Scan.Z1 and analyzed using Zen Blue 2.3 software. The regions of interest were analyzed for quantifying the total vessel length using the distance tool.

#### RNA isolation/NanoString profiling

miRNA expression analysis was performed using the NanoString nCounter miRNA expression assays (NanoString Technologies, Seattle, WA). Matched areas ( $2 \times 10^6 \mu\text{m}^2$ ) of ipsilateral peri-infarct area or contralateral peri-infarct area were laser captured, catapulted into lysis buffer, using a laser capture microdissection (LCM) system (Zeiss PALM Technologies, Germany) as described previously by our group.<sup>6,8,74,79–81</sup> Briefly, OCT-embedded brain tissue samples were cut into 12-µm-thick sections, stained with hematoxylin and eosin (H&E), washed with DEPC-H<sub>2</sub>O, dehydrated in ethanol, cut, and captured as described.<sup>80</sup> For LCM captures involving specific cell populations, the sections were stained with anti-NeuN (Abcam; ab190565), anti-GFAP (Abcam; ab49874), or anti-CD31 (Invitrogen; 12-0311-83) antibodies (1:50) for 30 min, subsequently washed with DEPC-H<sub>2</sub>O, and dehydrated in ethanol. Stained cells were catapulted into 25 µL of cell direct lysis extraction buffer (Invitrogen). Approximately 300–500 cells were captured per sample into each cap, and cDNA synthesis from the lysate was achieved using a Superscript Vilo cDNA synthesis kit (Thermo Fisher Scientific). RNA from LCM samples was isolated using the Total RNA Purification Micro Kit (Norgen Biotek, Thorold, ON, Canada). RNA quality was checked as described previously.<sup>80,82</sup> For NanoString profiling, total RNA (100 ng) was used as input material, and the assay was performed according to the manufacturer's instructions (NanoString Technologies, Seattle, WA). miRNA abundance was quantified using the NanoString mouse miRNA v.1.2 panel, which profiled 598 unique mature miRNAs. Quality control, normalization, and data analysis were performed using nSolver Analysis software (NanoString Technologies). Internal negative control probes included in each assay were used to determine a background threshold (3 SD above the mean negative control probe count value) for each sample. Background was subtracted from raw count values for each probe. Positive control count values were then used to normalize samples for any differences in sample preparation, hybridization, and Prep Station processing efficiency. Additional data analysis was performed using Genespring GX (Agilent Technologies, Santa Clara, CA). All differentially expressed miR were identified using t test with a significance level set at  $p < 0.05$ .<sup>2,81,83</sup>

#### Ingenuity Pathway Analysis

The biological functions of differentially expressed TCT-sensitive upregulated (contralateral versus peri-infarct) microRNAs were analyzed using IPA (Ingenuity Systems) as described previously.<sup>84–86</sup> Briefly, the Excel file containing the list of differentially expressed microRNAs was loaded as a dataset in the IPA software. Core analysis was then performed to obtain enriched pathways represented by microRNAs using the Ingenuity Knowledge Base with default settings in IPA. Both direct and indirect relationships that could affect networks and upstream regulators were considered. A total of seven bio-functions were significantly enriched by miR-1224 and miR-770

( $p < 0.05$ ). miR-1224 was the only miR that was involved in sprouting angiogenesis ( $p = 0.007$ ).<sup>87</sup> The IPA pathway tool was then used to generate a graphical representation of the biological relationships between differentially expressed miRs and biofunctions, where nodes represented genes and edges represented the biological functions.

#### Cell culture

Mouse pMBMECs were purchased from Cell Biologics (Chicago, IL; cat. no. C57-6023) and cultured according to the manufacturer's protocol. Briefly, pMBMECs were grown on pre-coated gelatin-based coating solution and maintained in a humidified incubator at 37°C with 5% CO<sub>2</sub> and 95% air. Mouse brain endothelial cells (bEnd.3, cat. no. CRL-2299; ATCC, Manassas, VA) were cultured in DMEM (Dulbecco's modified Eagle's medium with 4,500 mg/L D-glucose, 1 mM sodium pyruvate, 1,500 mg/L sodium bicarbonate; ATCC, Manassas, VA) supplemented with 10% fetal bovine serum, 100 µg/mL streptomycin, 100 U/mL penicillin, and 0.25 µg/mL amphotericin (all from Thermo Fisher Scientific). bEnd.3 cells were maintained in a humidified incubator at 37°C with 5% CO<sub>2</sub> and 95% air.

#### In vitro transfection of miR mimic or siRNA

bEnd.3 cells ( $0.12 \times 10^6$  cells/well in 12 well plates) or primary brain microvascular cells ( $0.2 \times 10^6$  cells/well in 12 well plates) were seeded in the medium for 18–24 h before transfection. DharmaFECT 1 transfection reagent was used to transfect cells with miRIDIAN mmu-miR-1224 mimic or SERPINE1 siRNA as described previously.<sup>6,12,73,74</sup> miRIDIAN miR mimic or siControl nontargeting siRNA pool (Thermo Fisher Scientific) was used for control transfections. Samples were collected after 72 h of miR mimic or siRNA transfection for quantification of miR, mRNA, or protein expression for the indicated time points as specified in the respective figure legends.

#### RNA isolation and quantitative real-time PCR for mRNA and miRNA

Total RNA was extracted using the total RNA extraction and purification isolation kit according to the manufacturer's protocol (Norgen Biotek, Thorold, ON, Canada). The mRNA expression levels of specific cell populations (NeuN, GFAP, and CD31) and the housekeeping control  $\beta$ -actin were quantified by quantitative real-time PCR using the PowerUp SYBR Green Master Mix. For gene expression studies, total cDNA synthesis was achieved using the SuperScript VILO cDNA synthesis kit (Thermo Fisher Scientific). For determination of miR expression, specific TaqMan assays for miRs and the TaqMan MicroRNA Reverse Transcription Kit were used, followed by real-time PCR using the Universal PCR Master Mix (Thermo Fisher Scientific). Levels of miRNA were quantified with the relative quantification method using U6 as the housekeeping miRNA. The abundance of mRNA for *Serpine1* was quantified by real-time PCR by using the PowerUp SYBR Green Master Mix. Gapdh served as housekeeping control. The following primer sets were used:

m\_Gapdh F: 5'-ATGACCACAGTCCATGCCATCACT-3'

m\_Gapdh R: 5'-TGTTGAAGTCGCAGGAGACAACCT-3'

m\_Serpine1 F: 5'-CCTCTTCCACAAGTCTGATGGCC-3'

m\_Serpine1 R: 5'-GCAGTTCCACAACGTCATACTCG-3'

m\_NeuN F: 5'-CCAGGCACTGAGGCCAGCAC-3'

m\_NeuN R: 5'-ACATTTGCCGCAGGTCGGGG-3'

m\_GFAP F: 5'-CACCTACAGGAAATTGCTGGAGG-3'

m\_GFAP R: 5'-CCACGATGTTCTCTTGAGGTG-3'

m\_CD31 F: 5'-CCAAAGCCAGTAGCATCATGGTC-3'

m\_CD31 R: 5'-GGATGGTGAAGTTGGCTACAGG-3'

m\_β-actin F: 5'-AGAGGGAAATCGTGCGTGAC-3'

m\_β-actin R: 5'-CAATAGTGATGACCTGGCCGT-3'

#### Matrigel tube formation assay

*In vitro* angiogenic responses were assessed by the tube-forming ability on Matrigel as described previously.<sup>79,86,88,89</sup> Briefly, endothelial cells were treated with TM5441 (10 µM) or transfected with controls, miR-1224 mimic, or SERPINE1 siRNA. Three days after transfection or 24 h after TM5441 treatment, the cells were seeded on Matrigel pre-coated four-well plates at  $8 \times 10^4$  cells/well. The angiogenic properties were assessed 8–10 h (bEnd.3 cells) or 24 h (primary endothelial cells) after plating on Matrigel. Images were acquired after the indicated period of time on a Leica DMi1 microscope (5× magnification; Leica Microsystems, Buffalo Grove, IL). All images of tube formation were analyzed using the pre-set Angiogenesis Analyzer plug-in tool of ImageJ analysis software.<sup>90–92</sup> The parameters evaluated were number of nodes (branching points), number of junctions (junctions with three or more furcated branches), number of meshes (the closed loops), and the total length of the capillary network.

#### Angiogenesis profiler array

Cell extracts collected from transfected bEnd.3 cells were subjected to a proteome profiler array using a mouse angiogenesis array kit (ARY015; R&D Systems, Minneapolis, MN). Briefly, for protein isolation, cell lysate was prepared by pooling six wells of a 12-well plate per sample. The array procedure and data analysis were performed according to the manufacturer's protocol. The arrays were imaged with an Azure Biosystems Imager c600 (Dublin, CA) and quantification of signal intensity was performed using ImageJ.

#### miR-target 3' UTR luciferase reporter assay

bEnd.3 cells ( $0.06 \times 10^6$  cells/well) were seeded in 24-well plates for 18–24 h before transfection. mimic-miR-1224 was transfected into bEnd.3 cells using the DharmaFECT 1 transfection reagent for 48 h, followed by transfection with SERPINE1 3' UTR plasmids using Lipofectamine 3000 (Thermo Fisher Scientific). *Gussia* luciferase (GLuc) activity and alkaline phosphatase activity were assayed after

48 h of transfection using GeneCopoeia's Secrete-Pair Dual Luminescence Assay Kit (LF031) according to the manufacturer's instructions. Percentage of GLuc activity was calculated after normalizing to alkaline phosphatase activity.

### Enzyme-linked immunosorbent assay

SERPINE1 levels were measured using a commercially available ELISA kit (DY3828-05; R&D Systems, Minneapolis, MN) following the manufacturer's protocol as previously described.<sup>93</sup>

### Statistical analyses

All statistical analyses were performed using GraphPad Prism software (version 9.0; GraphPad Software, San Diego, CA). The  $\Delta\Delta Ct$  value was used for statistical analysis of all quantitative real-time PCR data. "n" indicates the sample size (mice) in each group. Data are presented as the mean  $\pm$  SE. Differences between means were tested using Student's t test or ANOVA followed by Sidak's multiple comparisons test as appropriate. A value of  $p < 0.05$  was considered statistically significant and exact p values are indicated in all relevant figures.

### SUPPLEMENTAL INFORMATION

Supplemental information can be found online at <https://doi.org/10.1016/j.omtn.2022.12.019>.

### ACKNOWLEDGMENTS

We thank the Indiana University Laboratory Animal Resource Center for the care of mice in accordance with National Institutes of Health (NIH) guidelines. We also thank Puneeth Khandelwal and Laura Zichella for helping us with the animal work and immunohistochemistry. This research was supported in part by the US National Institutes of Health, National Institute of Neurological Disorders and Stroke grant R01NS042617 (C.K.S. and S.K.). It was also supported by R01NS085272 and Department of Defense grant W81XWH-21-1-0047 to S.K. The work was supported by Lilly Indiana Collaborative Initiative for Talent Enrichment (INCITE) fellowships to C.K.S. as well as to S.R. This study was supported by NIH R01 GM069589, GM077185, GM108014, DK128845, DK125835, and NR013898 to C.K.S. and in part by NIH DK076566 to S.R.

### AUTHOR CONTRIBUTIONS

Conceptualization, S.K. and C.K.S.; methodology, N.B., R.P., S.C.G., M.S., K.S., S.G., S.R., S.K., and C.K.S.; investigation and validation, R.P., N.B., S.C.G., S.R., and S.K.; formal analysis, R.P., S.R., S.K., and K.S.; writing – original draft, R.P., C.K.S., and S.K.; visualization, C.K.S., S.R., S.G., and S.K.; funding acquisition, S.K. and C.K.S.; resources, S.R., S.K., and C.K.S.; supervision, S.R., C.K.S., and S.K.

### REFERENCES

- George, M.G., Fischer, L., Koroshetz, W., Bushnell, C., Frankel, M., Foltz, J., and Thorpe, P.G. (2017). CDC grand rounds: public health strategies to prevent and treat strokes. *MMWR Morb. Mortal. Wkly. Rep.* 66, 479–481. <https://doi.org/10.15585/mmwr.mm6618a5>.
- Powers, C.J., Dickerson, R., Zhang, S.W., Rink, C., Roy, S., and Sen, C.K. (2016). Human cerebrospinal fluid microRNA: temporal changes following subarachnoid hemorrhage. *Physiol. Genomics* 48, 361–366. <https://doi.org/10.1152/physiolgenomics.00052.2015>.
- Sen, C.K., Khanna, S., Roy, S., and Packer, L. (2000). Molecular basis of vitamin E action. Tocotrienol potently inhibits glutamate-induced pp60(c-Src) kinase activation and death of HT4 neuronal cells. *J. Biol. Chem.* 275, 13049–13055. <https://doi.org/10.1074/jbc.275.17.13049>.
- Sen, C.K., Khanna, S., and Roy, S. (2007). Tocotrienols in health and disease: the other half of the natural vitamin E family. *Mol. Aspects Med.* 28, 692–728. <https://doi.org/10.1016/j.mam.2007.03.001>.
- Khanna, S., Heigel, M., Weist, J., Gnyawali, S., Teplitsky, S., Roy, S., Sen, C.K., and Rink, C. (2015). Excessive alpha-tocopherol exacerbates microglial activation and brain injury caused by acute ischemic stroke. *FASEB J* 29, 828–836. <https://doi.org/10.1096/fj.14-263723>.
- Khanna, S., Rink, C., Ghoorkhanian, R., Gnyawali, S., Heigel, M., Wijesinghe, D.S., Chalfant, C.E., Chan, Y.C., Banerjee, J., Huang, Y., et al. (2013). Loss of miR-29b following acute ischemic stroke contributes to neural cell death and infarct size. *J. Cereb. Blood Flow Metab.* 33, 1197–1206. <https://doi.org/10.1038/jcbfm.2013.68>.
- Khanna, S., Roy, S., Slivka, A., Craft, T.K.S., Chaki, S., Rink, C., Notestine, M.A., DeVries, A.C., Parinandi, N.L., and Sen, C.K. (2005). Neuroprotective properties of the natural vitamin E alpha-tocotrienol. *Stroke* 36, 2258–2264. <https://doi.org/10.1161/01.STR.0000181082.70763.22>.
- Park, H.A., Kubicki, N., Gnyawali, S., Chan, Y.C., Roy, S., Khanna, S., and Sen, C.K. (2011). Natural vitamin E alpha-tocotrienol protects against ischemic stroke by induction of multidrug resistance-associated protein 1. *Stroke* 42, 2308–2314. <https://doi.org/10.1161/STROKEAHA.110.608547>.
- Rink, C., Christoforidis, G., Khanna, S., Peterson, L., Patel, Y., Khanna, S., Abduljalil, A., Irfanoglu, O., Machiraju, R., Bergdall, V.K., and Sen, C.K. (2011). Tocotrienol vitamin E protects against preclinical canine ischemic stroke by inducing arteriogenesis. *J. Cereb. Blood Flow Metab.* 31, 2218–2230. <https://doi.org/10.1038/jcbfm.2011.85>.
- Slivka, A., Rink, C., Paoletto, D., and Sen, C.K. (2020). Platelet function in stroke/transient ischemic attack patients treated with tocotrienol. *FASEB J* 34, 11838–11843. <https://doi.org/10.1096/fj.201902216RR>.
- Khanna, S., Parinandi, N.L., Kotha, S.R., Roy, S., Rink, C., Bibus, D., and Sen, C.K. (2010). Nanomolar vitamin E alpha-tocotrienol inhibits glutamate-induced activation of phospholipase A2 and causes neuroprotection. *J. Neurochem.* 112, 1249–1260. <https://doi.org/10.1111/j.1471-4159.2009.06550.x>.
- Khanna, S., Roy, S., Park, H.A., and Sen, C.K. (2007). Regulation of c-Src activity in glutamate-induced neurodegeneration. *J. Biol. Chem.* 282, 23482–23490. <https://doi.org/10.1074/jbc.M611269200>.
- Sen, C.K., Rink, C., and Khanna, S. (2010). Palm oil-derived natural vitamin E alpha-tocotrienol in brain health and disease. *J. Am. Coll. Nutr.* 29, 314S–323S. <https://doi.org/10.1080/07315724.2010.10719846>.
- Christoforidis, G.A., Rink, C., Kontzialis, M.S., Mohammad, Y., Koch, R.M., Abduljalil, A.M., Bergdall, V.K., Roy, S., Khanna, S., Slivka, A.P., et al. (2011). An endovascular canine middle cerebral artery occlusion model for the study of leptomeningeal collateral recruitment. *Invest. Radiol.* 46, 34–40. <https://doi.org/10.1097/RLI.0b013e3181f0cbc7>.
- Rink, C., Christoforidis, G., Abduljalil, A., Kontzialis, M., Bergdall, V., Roy, S., Khanna, S., Slivka, A., Knopp, M., and Sen, C.K. (2008). Minimally invasive neuroradiologic model of preclinical transient middle cerebral artery occlusion in canines. *Proc. Natl. Acad. Sci. USA* 105, 14100–14105. <https://doi.org/10.1073/pnas.0806678105>.
- Lin, M.P., and Liebeskind, D.S. (2016). Imaging of ischemic stroke. *Continuum* 22, 1399–1423. <https://doi.org/10.1212/CON.0000000000000376>.
- Menon, B.K., and Goyal, M. (2015). Imaging paradigms in acute ischemic stroke: a pragmatic evidence-based approach. *Radiology* 277, 7–12. <https://doi.org/10.1148/radiol.2015151030>.
- Grefkes, C., and Fink, G.R. (2020). Recovery from stroke: current concepts and future perspectives. *Neurol. Res. Pract.* 2, 17.

19. Niu, Y., Mo, D., Qin, L., Wang, C., Li, A., Zhao, X., Wang, X., Xiao, S., Wang, Q., Xie, Y., et al. (2011). Lipopolysaccharide-induced miR-1224 negatively regulates tumour necrosis factor- $\alpha$  gene expression by modulating Sp1. *Immunology* *133*, 8–20. <https://doi.org/10.1111/j.1365-2567.2010.03374.x>.
20. Granados-Durán, P., López-Ávalos, M.D., Grondona, J.M., Gómez-Roldán, M.D.C., Cifuentes, M., Pérez-Martín, M., Alvarez, M., Rodríguez de Fonseca, F., and Fernández-Llebrez, P. (2015). Neuroinflammation induced by intracerebroventricular injection of microbial neuraminidase. *Front. Med.* *2*, 14. <https://doi.org/10.3389/fmed.2015.00014>.
21. Tejedor, L.S., Wostradowski, T., Gingele, S., Skripuletz, T., Gudi, V., and Stangel, M. (2017). The effect of stereotactic injections on demyelination and remyelination: a study in the cuprizone model. *J. Mol. Neurosci.* *61*, 479–488. <https://doi.org/10.1007/s12031-017-0888-y>.
22. Wallace, M.N., and Fredens, K. (1992). Activated astrocytes of the mouse hippocampus contain high levels of NADPH-diaphorase. *Neuroreport* *3*, 953–956. <https://doi.org/10.1097/00001756-199211000-00001>.
23. Chen, Y., and Wang, X. (2020). miRDB: an online database for prediction of functional microRNA targets. *Nucleic Acids Res.* *48*, D127–D131. <https://doi.org/10.1093/nar/gkz757>.
24. Enright, A.J., John, B., Gaul, U., Tuschl, T., Sander, C., and Marks, D.S. (2003). MicroRNA targets in *Drosophila*. *Genome Biol.* *5*, R1. <https://doi.org/10.1186/gb-2003-5-1-r1>.
25. Loher, P., and Rigoutsos, I. (2012). Interactive exploration of RNA22 microRNA target predictions. *Bioinformatics* *28*, 3322–3323. <https://doi.org/10.1093/bioinformatics/bts615>.
26. McGeary, S.E., Lin, K.S., Shi, C.Y., Pham, T.M., Bisaria, N., Kelley, G.M., and Bartel, D.P. (2019). The biochemical basis of microRNA targeting efficacy. *Science* *366*, eaav1741. <https://doi.org/10.1126/science.aav1741>.
27. Sticht, C., De La Torre, C., Parveen, A., and Gretz, N. (2018). miRWalk: An online resource for prediction of microRNA binding sites. *PLoS One* *13*, e0206239. <https://doi.org/10.1371/journal.pone.0206239>.
28. Boe, A.E., Eren, M., Murphy, S.B., Kamide, C.E., Ichimura, A., Terry, D., McAnally, D., Smith, L.H., Miyata, T., and Vaughan, D.E. (2013). Plasminogen activator inhibitor-1 antagonist TM5441 attenuates Nomega-nitro-L-arginine methyl ester-induced hypertension and vascular senescence. *Circulation* *128*, 2318–2324. <https://doi.org/10.1161/CIRCULATIONAHA.113.003192>.
29. Wang, D., Yang, L.Y., Liu, Z., Yu, J., Zhang, M.J., Zhang, Y., Cai, Y., Xu, X., Hao, J.J., and Wang, M.R. (2020). PAI-1 overexpression promotes invasion and migration of esophageal squamous carcinoma cells. *Yi Chuan* *42*, 287–295. <https://doi.org/10.16288/j.ycz.19-334>.
30. Chan, S.L., Bishop, N., Li, Z., and Cipolla, M.J. (2018). Inhibition of PAI (plasminogen activator inhibitor)-1 improves brain collateral perfusion and injury after acute ischemic stroke in aged hypertensive rats. *Stroke* *49*, 1969–1976. <https://doi.org/10.1161/STROKEAHA.118.022056>.
31. Fisher, M.J. (2013). Brain regulation of thrombosis and hemostasis: from theory to practice. *Stroke* *44*, 3275–3285. <https://doi.org/10.1161/STROKEAHA.113.000736>.
32. Petersen, M.A., Ryu, J.K., and Akassoglou, K. (2018). Fibrinogen in neurological diseases: mechanisms, imaging and therapeutics. *Nat. Rev. Neurosci.* *19*, 283–301. <https://doi.org/10.1038/nrn.2018.13>.
33. Thiebaut, A.M., Gauberti, M., Ali, C., Martinez De Lizarondo, S., Vivien, D., Yepes, M., and Roussel, B.D. (2018). The role of plasminogen activators in stroke treatment: fibrinolysis and beyond. *Lancet Neurol.* *17*, 1121–1132. [https://doi.org/10.1016/S1474-4422\(18\)30323-5](https://doi.org/10.1016/S1474-4422(18)30323-5).
34. Stankovic, S., and Majkic-Singh, N. (2010). Genetic aspects of ischemic stroke: coagulation, homocysteine, and lipoprotein metabolism as potential risk factors. *Crit. Rev. Clin. Lab. Sci.* *47*, 72–123. <https://doi.org/10.3109/10408361003791520>.
35. Rehnström, M., Frederiksen, S.D., Ansar, S., and Edvinsson, L. (2020). Transcriptome profiling revealed early vascular smooth muscle cell gene activation following focal ischemic stroke in female rats - comparisons with males. *BMC Genom.* *21*, 883. <https://doi.org/10.1186/s12864-020-07295-2>.
36. Griemert, E.V., Recarte Pelz, K., Engelhard, K., Schäfer, M.K., and Thal, S.C. (2019). PAI-1 but not PAI-2 gene deficiency attenuates ischemic brain injury after experimental stroke. *Transl. Stroke Res.* *10*, 372–380. <https://doi.org/10.1007/s12975-018-0644-9>.
37. Li, D.D., Pang, H.G., Song, J.N., Zhao, Y.L., Zhang, B.F., Ma, X.D., and Sun, P. (2015). Receptor-associated protein promotes t-PA expression, reduces PAI-1 expression and improves neurorecovery after acute ischemic stroke. *J. Neurol. Sci.* *350*, 84–89. <https://doi.org/10.1016/j.jns.2015.02.022>.
38. Pu, Z., Bao, X., Xia, S., Shao, P., and Xu, Y. (2022). Serpine1 regulates peripheral neutrophil recruitment and acts as potential target in ischemic stroke. *J. Inflamm. Res.* *15*, 2649–2663. <https://doi.org/10.2147/JIR.S361072>.
39. Maes, M., Nikiforov, N.G., Plaimas, K., Suratane, A., Alfieri, D.F., and Vissoci Reiche, E.M. (2021). New drug targets to prevent death due to stroke: a review based on results of protein-protein interaction network, enrichment, and annotation analyses. *Int. J. Mol. Sci.* *22*, 12108. <https://doi.org/10.3390/ijms222212108>.
40. Bruno, G., Ritelli, M., Di Pietro, A., Cipriano, L., Colombi, M., Lus, G., and Puoti, G. (2021). Clinical and genetic heterogeneity in a large family with pseudoaxanthoma elasticum: MTHFR and SERPINE1 variants as possible disease modifiers in developing ischemic stroke. *J. Stroke Cerebrovasc. Dis.* *30*, 105744. <https://doi.org/10.1016/j.jstrokecerebrovasdis.2021.105744>.
41. Dong, W., and Wu, X. (2018). Overexpression of Rab11-FIP2 in colorectal cancer cells promotes tumor migration and angiogenesis through increasing secretion of PAI-1. *Cancer Cell Int.* *18*, 35. <https://doi.org/10.1186/s12935-018-0532-0>.
42. Geis, T., Döring, C., Popp, R., Grossmann, N., Fleming, I., Hansmann, M.L., Dehne, N., and Brüne, B. (2015). HIF-2 $\alpha$ -dependent PAI-1 induction contributes to angiogenesis in hepatocellular carcinoma. *Exp. Cell Res.* *331*, 46–57. <https://doi.org/10.1016/j.yexcr.2014.11.018>.
43. Takayama, Y., Hattori, N., Hamada, H., Masuda, T., Omori, K., Akita, S., Iwamoto, H., Fujitaka, K., and Kohno, N. (2016). Inhibition of PAI-1 limits tumor angiogenesis regardless of angiogenic stimuli in malignant pleural mesothelioma. *Cancer Res.* *76*, 3285–3294. <https://doi.org/10.1158/0008-5472.CAN-15-1796>.
44. Teng, F., Zhang, J.X., Chen, Y., Shen, X.D., Su, C., Guo, Y.J., Wang, P.H., Shi, C.C., Lei, M., Cao, Y.O., and Liu, S.Q. (2021). LncRNA NKX2-1-AS1 promotes tumor progression and angiogenesis via upregulation of SERPINE1 expression and activation of the VEGFR-2 signaling pathway in gastric cancer. *Mol. Oncol.* *15*, 1234–1255. <https://doi.org/10.1002/1878-0261.12911>.
45. Li, S., Wei, X., He, J., Tian, X., Yuan, S., and Sun, L. (2018). Plasminogen activator inhibitor-1 in cancer research. *Biomed. Pharmacother.* *105*, 83–94. <https://doi.org/10.1016/j.biopha.2018.05.119>.
46. Providence, K.M., Higgins, S.P., Mullen, A., Battista, A., Samarakoon, R., Higgins, C.E., Wilkins-Port, C.E., and Higgins, P.J. (2008). SERPINE1 (PAI-1) is deposited into keratinocyte migration “trails” and required for optimal monolayer wound repair. *Arch. Dermatol. Res.* *300*, 303–310. <https://doi.org/10.1007/s00403-008-0845-2>.
47. Qi, L., Higgins, S.P., Lu, Q., Samarakoon, R., Wilkins-Port, C.E., Ye, Q., Higgins, C.E., Staiano-Coico, L., and Higgins, P.J. (2008). SERPINE1 (PAI-1) is a prominent member of the early G0  $\rightarrow$  G1 transition “wound repair” transcriptome in p53 mutant human keratinocytes. *J. Invest. Dermatol.* *128*, 749–753. <https://doi.org/10.1038/sj.jid.571068>.
48. McCann, J.V., Xiao, L., Kim, D.J., Khan, O.F., Kowalski, P.S., Anderson, D.G., Pecot, C.V., Azam, S.H., Parker, J.S., Tsai, Y.S., et al. (2019). Endothelial miR-30c suppresses tumor growth via inhibition of TGF- $\beta$ -induced Serpine1. *J. Clin. Invest.* *129*, 1654–1670. <https://doi.org/10.1172/JCI123106>.
49. Aillaud, M.F., Pignol, F., Alessi, M.C., Harle, J.R., Escande, M., Mongin, M., and Juhan-Vague, I. (1986). Increase in plasma concentration of plasminogen activator inhibitor, fibrinogen, von Willebrand factor, factor VIII: C and in erythrocyte sedimentation rate with age. *Thromb. Haemost.* *55*, 330–332.
50. Howe, G.A., Kazda, K., and Addison, C.L. (2017). MicroRNA-30b controls endothelial cell capillary morphogenesis through regulation of transforming growth factor  $\beta$  2. *PLoS One* *12*, e0185619. <https://doi.org/10.1371/journal.pone.0185619>.
51. Marchand, A., Proust, C., Morange, P.E., Lompré, A.M., and Tréguët, D.A. (2012). miR-421 and miR-30c inhibit SERPINE 1 gene expression in human endothelial cells. *PLoS One* *7*, e44532. <https://doi.org/10.1371/journal.pone.0044532>.

52. Wang, W., and Jia, L. (2021). Regulatory mechanism of MicroRNA-30b on neonatal hypoxic-ischemic encephalopathy (HIE). *J. Stroke Cerebrovasc. Dis.* 30, 105553. <https://doi.org/10.1016/j.jstrokecerebrovasdis.2020.105553>.
53. Cohen, C., Le Goff, O., Soysouvanh, F., Vasseur, F., Tanou, M., Nguyen, C., Amrouche, L., Le Guen, J., Saltel-Fulero, O., Meunier, T., et al. (2021). Glomerular endothelial cell senescence drives age-related kidney disease through PAI-1. *EMBO Mol. Med.* 13, e14146. <https://doi.org/10.15252/emmm.202114146>.
54. Carratala, A., Martinez-Hervas, S., Rodriguez-Borja, E., Benito, E., Real, J.T., Saez, G.T., Carmena, R., and Ascaso, J.F. (2018). PAI-1 levels are related to insulin resistance and carotid atherosclerosis in subjects with familial combined hyperlipidemia. *J. Investig. Med.* 66, 17–21. <https://doi.org/10.1136/jim-2017-000468>.
55. Furukawa, S., Fujita, T., Shimabukuro, M., Iwaki, M., Yamada, Y., Nakajima, Y., Nakayama, O., Makishima, M., Matsuda, M., and Shimomura, I. (2004). Increased oxidative stress in obesity and its impact on metabolic syndrome. *J. Clin. Invest.* 114, 1752–1761. <https://doi.org/10.1172/JCI21625>.
56. Meltzer, M.E., Lisman, T., de Groot, P.G., Meijers, J.C.M., le Cessie, S., Doggen, C.J.M., and Rosendaal, F.R. (2010). Venous thrombosis risk associated with plasma hypofibrinolysis is explained by elevated plasma levels of TAFI and PAI-1. *Blood* 116, 113–121. <https://doi.org/10.1182/blood-2010-02-267740>.
57. Basisty, N., Kale, A., Jeon, O.H., Kuehnemann, C., Payne, T., Rao, C., Holtz, A., Shah, S., Sharma, V., Ferrucci, L., et al. (2020). A proteomic atlas of senescence-associated secretomes for aging biomarker development. *PLoS Biol.* 18, e3000599. <https://doi.org/10.1371/journal.pbio.3000599>.
58. Martins, S.R., Toledo, S.L.d.O., da Silva, A.J., Mendes, F.S., de Oliveira, M.M., Ferreira, L.G.R., Dusse, L.M.S., Carvalho, M.D.G., Rios, D.R.A., Alpoim, P.N., and Pinheiro, M.d.B. (2022). Endothelial dysfunction biomarkers in sickle cell disease: is there a role for ADMA and PAI-1? *Ann. Hematol.* 101, 273–280. <https://doi.org/10.1007/s00277-021-04695-6>.
59. Han, M., and Pandey, D. (2021). ZMPSTE24 regulates SARS-CoV-2 spike protein-enhanced expression of endothelial PAI-1. *Am. J. Respir. Cell Mol. Biol.* 65, 300–308. <https://doi.org/10.1165/rccb.2020-0544OC>.
60. Katta, S., Karnear, S., Panuganti, D., Jerald, M.K., Sastry, B.K.S., and Kotamraju, S. (2018). Mitochondria-targeted esculetin inhibits PAI-1 levels by modulating STAT3 activation and miR-19b via SIRT3: role in acute coronary artery syndrome. *J. Cell. Physiol.* 233, 214–225. <https://doi.org/10.1002/jcp.25865>.
61. Kang, S., Tanaka, T., Inoue, H., Ono, C., Hashimoto, S., Kioi, Y., Matsumoto, H., Matsuura, H., Matsubara, T., Shimizu, K., et al. (2020). IL-6 trans-signaling induces plasminogen activator inhibitor-1 from vascular endothelial cells in cytokine release syndrome. *Proc. Natl. Acad. Sci. USA* 117, 22351–22356. <https://doi.org/10.1073/pnas.2010229117>.
62. Li, L., Wang, Y., Yu, X., Bao, Y., An, L., Wei, X., Yu, W., Liu, B., Li, J., Yang, J., et al. (2020). Bone marrow mesenchymal stem cell-derived exosomes promote plasminogen activator inhibitor 1 expression in vascular cells in the local microenvironment during rabbit osteonecrosis of the femoral head. *Stem Cell Res. Ther.* 11, 480. <https://doi.org/10.1186/s13287-020-01991-2>.
63. Wu, Y., Chen, Z., Wang, Y., and Peng, F. (2020). MiR-3691-5p is upregulated in docosahexaenoic acid-treated vascular endothelial cell and targets serpin family E member 1. *J. Cell. Biochem.* 121, 2363–2371. <https://doi.org/10.1002/jcb.29459>.
64. Chen, Y., Yang, C., Li, Y., Chen, L., Yang, Y., Belguise, K., Wang, X., Lu, K., and Yi, B. (2019). MiR145-5p inhibits proliferation of PMVECs via PAI-1 in experimental hepato-pulmonary syndrome rat pulmonary microvascular hyperplasia. *Biol. Open* 8, bio044800.
65. Patel, N., Tahara, S.M., Malik, P., and Kalra, V.K. (2011). Involvement of miR-30c and miR-301a in immediate induction of plasminogen activator inhibitor-1 by placental growth factor in human pulmonary endothelial cells. *Biochem. J.* 434, 473–482. <https://doi.org/10.1042/BJ20110585>.
66. Osada-Oka, M., Shiota, M., Izumi, Y., Nishiyama, M., Tanaka, M., Yamaguchi, T., Sakurai, E., Miura, K., and Iwao, H. (2017). Macrophage-derived exosomes induce inflammatory factors in endothelial cells under hypertensive conditions. *Hypertens. Res.* 40, 353–360. <https://doi.org/10.1038/hr.2016.163>.
67. Gonsalves, C.S., Li, C., Malik, P., Tahara, S.M., and Kalra, V.K. (2015). Peroxisome proliferator-activated receptor- $\alpha$ -mediated transcription of miR-301a and miR-454 and their host gene SKA2 regulates endothelin-1 and PAI-1 expression in sickle cell disease. *Biosci. Rep.* 35, e00275. <https://doi.org/10.1042/BSR20150190>.
68. Gopalan, Y., Shuaib, I.L., Magosso, E., Ansari, M.A., Abu Bakar, M.R., Wong, J.W., Khan, N.A.K., Liong, W.C., Sundram, K., Ng, B.H., et al. (2014). Clinical investigation of the protective effects of palm vitamin E tocotrienols on brain white matter. *Stroke* 45, 1422–1428. <https://doi.org/10.1161/STROKEAHA.113.004449>.
69. Garcia, V., Park, E.J., Siragusa, M., Frohlich, F., Mahfuzul Haque, M., Pascale, J.V., Heberlein, K.R., Isakson, B.E., Stuehr, D.J., and Sessa, W.C. (2020). Unbiased proteomics identifies plasminogen activator inhibitor-1 as a negative regulator of endothelial nitric oxide synthase. *Proc. Natl. Acad. Sci. USA* 117, 9497–9507. <https://doi.org/10.1073/pnas.1918761117>.
70. Smith, T.L., Oubaha, M., Cagnone, G., Boscher, C., Kim, J.S., El Bakkouri, Y., Zhang, Y., Chidiac, R., Corriveau, J., Delisle, C., et al. (2021). eNOS controls angiogenic sprouting and retinal neovascularization through the regulation of endothelial cell polarity. *Cell. Mol. Life Sci.* 79, 37. <https://doi.org/10.1007/s00018-021-04042-y>.
71. Asahi, M., Huang, Z., Thomas, S., Yoshimura, S.I., Sumii, T., Mori, T., Qiu, J., Amin-Hanjani, S., Huang, P.L., Liao, J.K., et al. (2005). Protective effects of statins involving both eNOS and tPA in focal cerebral ischemia. *J. Cereb. Blood Flow Metab.* 25, 722–729. <https://doi.org/10.1038/sj.jcbfm.9600070>.
72. Kang, H.J., Kang, W.S., Hong, M.H., Choe, N., Kook, H., Jeong, H.C., Kang, J., Hur, J., Jeong, M.H., Kim, Y.S., and Ahn, Y. (2015). Involvement of miR-34c in high glucose-insulted mesenchymal stem cells leads to inefficient therapeutic effect on myocardial infarction. *Cell. Signal.* 27, 2241–2251. <https://doi.org/10.1016/j.cellsig.2015.07.024>.
73. Khanna, S., Stewart, R., Gnyawali, S., Harris, H., Balch, M., Spieldenner, J., Sen, C.K., and Rink, C. (2017). Phytoestrogen isoflavone intervention to engage the neuroprotective effect of glutamate oxaloacetate transaminase against stroke. *FASEB J* 31, 4533–4544. <https://doi.org/10.1096/fj.201700353>.
74. Rink, C., Gnyawali, S., Peterson, L., and Khanna, S. (2011). Oxygen-inducible glutamate oxaloacetate transaminase as protective switch transforming neurotoxic glutamate to metabolic fuel during acute ischemic stroke. *Antioxid. Redox Signal.* 14, 1777–1785. <https://doi.org/10.1089/ars.2011.3930>.
75. Rink, C., Gnyawali, S., Stewart, R., Teplitsky, S., Harris, H., Roy, S., Sen, C.K., and Khanna, S. (2017). Glutamate oxaloacetate transaminase enables anaplerotic refilling of TCA cycle intermediates in stroke-affected brain. *FASEB J* 31, 1709–1718. <https://doi.org/10.1096/fj.201601033R>.
76. Lemmerman, L.R., Balch, M.H.H., Moore, J.T., Alzate-Correa, D., Rincon-Benavides, M.A., Salazar-Puerta, A., Gnyawali, S., Harris, H.N., Lawrence, W., Ortega-Pineda, L., et al. (2021). Nanotransfection-based vasculogenic cell reprogramming drives functional recovery in a mouse model of ischemic stroke. *Sci. Adv.* 7. <https://doi.org/10.1126/sciadv.abd4735>.
77. Park, H.A., Khanna, S., Rink, C., Gnyawali, S., Roy, S., and Sen, C.K. (2009). Glutathione disulfide induces neural cell death via a 12-lipoxygenase pathway. *Cell Death Differ.* 16, 1167–1179. <https://doi.org/10.1038/cdd.2009.37>.
78. Robertson, R.T., Levine, S.T., Haynes, S.M., Gutierrez, P., Baratta, J.L., Tan, Z., and Longmuir, K.J. (2015). Use of labeled tomato lectin for imaging vasculature structures. *Histochem. Cell Biol.* 143, 225–234. <https://doi.org/10.1007/s00418-014-1301-3>.
79. Chan, Y.C., Roy, S., Khanna, S., and Sen, C.K. (2012). Downregulation of endothelial microRNA-200b supports cutaneous wound angiogenesis by desilencing GATA binding protein 2 and vascular endothelial growth factor receptor 2. *Arterioscler. Thromb. Vasc. Biol.* 32, 1372–1382. <https://doi.org/10.1161/ATVBAHA.112.248583>.
80. Kuhn, D.E., Roy, S., Radtke, J., Khanna, S., and Sen, C.K. (2007). Laser microdissection and capture of pure cardiomyocytes and fibroblasts from infarcted heart regions: perceived hyperoxia induces p21 in peri-infarct myocytes. *Am. J. Physiol. Heart Circ. Physiol.* 292, H1245–H1253. <https://doi.org/10.1152/ajpheart.01069.2006>.
81. Roy, S., Khanna, S., Hussain, S.R.A., Biswas, S., Azad, A., Rink, C., Gnyawali, S., Shilo, S., Nuovo, G.J., and Sen, C.K. (2009). MicroRNA expression in response to murine myocardial infarction: miR-21 regulates fibroblast metalloprotease-2 via phosphatase and tensin homologue. *Cardiovasc. Res.* 82, 21–29. <https://doi.org/10.1093/cvr/cvp015>.
82. Rink, C., Roy, S., Khan, M., Ananth, P., Kuppusamy, P., Sen, C.K., and Khanna, S. (2010). Oxygen-sensitive outcomes and gene expression in acute ischemic stroke. *J. Cereb. Blood Flow Metab.* 30, 1275–1287. <https://doi.org/10.1038/jcbfm.2010.7>.

83. Roy, S., Patel, D., Khanna, S., Gordillo, G.M., Biswas, S., Friedman, A., and Sen, C.K. (2007). Transcriptome-wide analysis of blood vessels laser captured from human skin and chronic wound-edge tissue. *Proc. Natl. Acad. Sci. USA* 104, 14472–14477. <https://doi.org/10.1073/pnas.0706793104>.
84. Rustagi, Y., Abouhashem, A.S., Verma, P., Verma, S.S., Hernandez, E., Liu, S., Kumar, M., Guda, P.R., Srivastava, R., Mohanty, S.K., et al. (2022). Endothelial phospholipase Cgamma2 improves outcomes of diabetic ischemic limb rescue following VEGF therapy. *Diabetes*. <https://doi.org/10.2337/db21-0830>.
85. Singh, K., Pal, D., Sinha, M., Ghatak, S., Gnyawali, S.C., Khanna, S., Roy, S., and Sen, C.K. (2017). Epigenetic modification of MicroRNA-200b contributes to diabetic vasculopathy. *Mol. Ther.* 25, 2689–2704. <https://doi.org/10.1016/j.ymthe.2017.09.009>.
86. Singh, K., Sinha, M., Pal, D., Tabasum, S., Gnyawali, S.C., Khona, D., Sarkar, S., Mohanty, S.K., Soto-Gonzalez, F., Khanna, S., et al. (2019). Cutaneous epithelial to mesenchymal transition activator ZEB1 regulates wound angiogenesis and closure in a glycemic status-dependent manner. *Diabetes* 68, 2175–2190. <https://doi.org/10.2337/db19-0202>.
87. Sakai, E., Miura, Y., Suzuki-Kouyama, E., Oka, K., Tachibana, M., Kawabata, K., Sakurai, F., and Mizuguchi, H. (2017). A mammalian mirtron miR-1224 promotes tube-formation of human primary endothelial cells by targeting anti-angiogenic factor epsin2. *Sci. Rep.* 7, 5541. <https://doi.org/10.1038/s41598-017-05782-3>.
88. Chan, Y.C., Khanna, S., Roy, S., and Sen, C.K. (2011). miR-200b targets Ets-1 and is down-regulated by hypoxia to induce angiogenic response of endothelial cells. *J. Biol. Chem.* 286, 2047–2056. <https://doi.org/10.1074/jbc.M110.158790>.
89. Shilo, S., Roy, S., Khanna, S., and Sen, C.K. (2008). Evidence for the involvement of miRNA in redox regulated angiogenic response of human microvascular endothelial cells. *Arterioscler. Thromb. Vasc. Biol.* 28, 471–477. <https://doi.org/10.1161/ATVBAHA.107.160655>.
90. Aksel, H., and Huang, G.T.J. (2017). Human and swine dental pulp stem cells form a vascularlike network after angiogenic differentiation in comparison with endothelial cells: a quantitative analysis. *J. Endod.* 43, 588–595. <https://doi.org/10.1016/j.joen.2016.11.015>.
91. Chevalier, F., Lavergne, M., Negroni, E., Ferratge, S., Carpentier, G., Gilbert-Sirieix, M., Siñeriz, F., Uzan, G., and Albanese, P. (2014). Glycosaminoglycan mimetic improves enrichment and cell functions of human endothelial progenitor cell colonies. *Stem Cell Res.* 12, 703–715. <https://doi.org/10.1016/j.scr.2014.03.001>.
92. Marquez-Curtis, L.A., Sultani, A.B., McGann, L.E., and Elliott, J.A.W. (2016). Beyond membrane integrity: assessing the functionality of human umbilical vein endothelial cells after cryopreservation. *Cryobiology* 72, 183–190. <https://doi.org/10.1016/j.cryobiol.2016.05.005>.
93. Das, A., Abas, M., Biswas, N., Banerjee, P., Ghosh, N., Rawat, A., Khanna, S., Roy, S., and Sen, C.K. (2019). A modified collagen dressing induces transition of inflammatory to reparative phenotype of wound macrophages. *Sci. Rep.* 9, 14293. <https://doi.org/10.1038/s41598-019-49435-z>.